Variation of Deep Water Formation in the Labrador Sea over the last glacial cycle (130 ky) and in future climate model projections

by

Melanie Cottet

Licence, University of Joseph Fourier, 1997
D.E.A., University of Joseph Fourier, 1999

A Dissertation Submitted in Partial Fulfillment of the
Requirements for the Degree of

Master in sciences

in the School of Earth and Ocean Sciences

[redacted] We accept this dissertation as conforming
to the required standard

[redacted]

Dr. A. J. Weaver, Supervisor (School of Earth and Ocean Sciences)

[redacted]

Dr. K. Telmer, Member (School of Earth and Ocean Sciences)

[redacted]

Dr. B. Hawkins, Outside Member (Department of Biology)

[redacted]

Dr. J. Fyfe, External Examiner (Canadian Centre for Climate modelling and analysis)

Supervisor: Dr. A. J. Weaver

Abstract

A major issue in paleoclimatology is understanding the exact relation between the gradual variations in solar forcing and geological records of rapid climate changes. The formation of North Atlantic Deep Water (NADW) tightly governs the present global climate and is believed to play a major role in this relation. In this thesis the variation of NADW formation from the last interglacial period (the Eemian - 125 kbp) to global warming projections is investigated using numerical simulations conducted with the UVic Earth System Climate Model. The results are compared with proxy paleo-reconstructions. The NADW is currently composed of two water masses: 1- the deep Denmark Strait Overflow Water (DSOW) originating from the Nordic Seas and represented in the model by convection in the Irminger Sea, 2- the intermediate Labrador Sea Water (LSW), seasonally renewed by winter convection.

In the different simulations it is seen that there is no convection in the Labrador Sea during the Eemian and the Last Glacial Maximum (LGM: 21 kbp) in agreement with paleo-reconstructions. The inception of modern-like circulation at 8 kbp proposed by these reconstructions is not captured by the model unless the fresh water forcing from ice sheet melting is applied in a transient simulation. This raises implications concerning the applicability of the use of equilibrium simulations in representing changing climates. In global warming projections, the formation of LSW stops as CO_2 rises, and recovers afterward. On the other hand, in all simulations the convection permanently remains active in the eastern North Atlantlic, its latitude depending on the sea ice edge position.

The convection occurs through the cooling of the North Atlantic Drift water. The Irminger convection site is in direct contact with the North Atlantic Drift and is therefore relatively stable. The LSW formation on the other hand takes place in a confined environment far from this source and is very sensitive to variations in surface fresh water fluxes. These variations can be induced by external forcings: CO_2 concentration and orbital geometry, as well as ice sheet melting.

It is seen that the intensity of the thermohaline circulation is highly dependent on LSW formation which hence plays a major role in the short term climate variations. This encourages further monitoring in the Labrador Sea as a measure of the oceanic response to anthropogenic warming.

Examiners:

[redacted]

Dr. A. J. Weaver, Supervisor (School of Earth and Ocean Sciences)

[redacted]

Dr. K. Telmer, Member (School of Earth and Ocean Sciences)

[redacted]

Dr. B. Hawkins, Outside Member (Department of Biology)

[redacted]

Dr. J. Fyfe, External Examiner (Canadian Centre for Climate modelling and analysis)

Acknowledgments

I gratefully acknowledge Dr. Andrew Weaver for welcoming me in the *Climate Modelling Group*, for his continuous encouragements and financial support.
I would like to thank Wanda Lewis for her constant practical and moral support as well as for the vital morning coffee.
I am indebted to many people especially our exceptional "Computer Administrator" Ed Wiebe for the much-needed and well-appreciated technical support, Mike Eby for his extensive help with the model, Michael Roth and Dáithí Stone for solving the endless LaTeX and Matlab problems I encountered, but mostly for patiently supporting me (also in the French meaning of the word: put up with me) during the writing process:

- Don't Panic, the answer is blowin' in the Wind -

I am deeply grateful to the "Climate Group" in general as well as to each individual person for creating such a dynamic work atmosphere.
Finally, but most importantly, I am thankful to my family and friends for always being there (thanks to the time difference for the 24 hours a days e-mail support...).

- merci -

"...le soleil en pleine figure nous laissâmes, pour quelques minutes, le monde poursuivre sa course autour de nous, sans nous en soucier..."

Milan Kundera, Risibles Amours

Table of Contents

List of Tables

List of Figures

Chapter 1

Introduction

1.1 Introduction

For the first time, we live at a point in history at which we are realising the impact of human activities on our environment. The more we become aware of climate variations, the more curious and worried we are about its future evolution and the global warming menace. Due to the burning of huge amounts of fossil fuels, we disturb the atmospheric composition out of its natural bounds. The increasing amount of greenhouse gases in the atmosphere modifies the Earth's energy radiation balance to the point of human perception. What consequences we are going to face in the next century remain unclear.
Models of the climate system, which are used to project future climate change, can only be compared with the present climate state which we have measured by a wide range of methods over the last few decades. But the climate system is not in equilibrium and paleoclimate studies provide opportunities to have a sense of radically different climate states. Based on various and sporadic proxy data, paleoclimatologists have built their understanding of the climate system and managed to reconstruct different climate states and transition mechanisms linking them. The recent improvements in numerical computation allow more detailed simulations of the global climate system, its different equilibrium states and their transition. Looking into the past and coordinating proxy data with model simulations, allows for the verification of these dynamical mechanisms and is a first step in validating the models before any confidence may be assigned to future predictions.

After the warm climate prevailing throughout the Cretaceous (100 My (million years ago)) and the major K/T crisis (65 My), the Earth underwent a long-term cooling trend during the Cenozoic (fig. 1.1). Geological features and orbital parameters produced favorable conditions for the birth of the recent ice-ages starting in the Quaternary. The first continental ice sheet developed in the Northern Hemisphere 2.5 My (Imbrie et al. 1992). Since then, as revealed by marine sediment and ice core isotope profiles, the climate has been oscillating between interglacial and glacial stages, first on a 41 ky (kilo years) cycle, then on a 100 ky cycle (Clark et al. 1999). Paleoclimate data support the Milankovitch theory which states that the glaciations are driven by changes in Earth's orbital parameters

with three distinct periodicities: eccentricity, 100 ky; obliquity, 41 ky; precession, 19-23 ky. However, shorter climate oscillations are the result of internal complex feedbacks within the atmosphere, ocean and cryosphere. Understanding how the climate reacts to these natural forcings is still a major unresolved issue in paleoclimatology.

The global ocean circulation, through its enormous heat capacity and inertia, plays a major role in regulating the climate. Deep sea sediment cores give access to a few properties of the ocean in the past, but remain sporadic in space and time. From these data, researchers try to reconstruct past ocean states. Complementary, modelling studies attempt to reproduce the full climate dynamics in order to understand mechanisms leading to these different oceanic states. Intercomparisons between model output and proxy data are essential for mechanistic validation to recompose the full climate story.

The purpose of this thesis is to compare model simulations and paleo-reconstructions conducted at the GEOTOP (Research Centre in Isotope Chemistry and Geochronology) by Hillaire-Marcel et al. (2001) and de Vernal et al. (2002). They focus on deep water formation in the Labrador Sea during two extreme climate states of the late Quaternary, namely the last interglacial period, 125 kbp (thousand years ago), and the Last Glacial Maximum (LGM), 21 kbp. The aim is to inquire about the deep water formation in the North Atlantic under different climate conditions prevailing through the last glacial cycle.

The study is based on model simulations conducted with the UVic Earth System Climate model. This model and the different simulations are described in chapter 2. In chapter 3, the focus is on two extreme climate states. First is the Eemian, 125 kbp, an interglacial stage supposedly warmer than today (White 1993). The second is the Last Glacial Maximum, 21 kbp, a cold period with the maximum continental ice sheet extension over North America and Eurasia. For each of these, proxy data obtained by microplankton analyses from Hillaire-Marcel et al. (2001) and de Vernal et al. (2002) are compared with the output of the model. In chapter 4, the hypothesis of Hillaire-Marcel et al. (2001), concerning the onset of deep water formation in the Labrador Sea around 8 kbp, is tested with integrations of more recent time periods in the Holocene. In chapter 5, future scenarios of global warming with high CO_2 concentrations are conducted to inquire about the evolution of the thermohaline circulation under a warming climate. The results are compared with Wood et al. (1999). First, to set the study in a larger context, the evolution of the late Quaternary climate and ocean circulation are described.

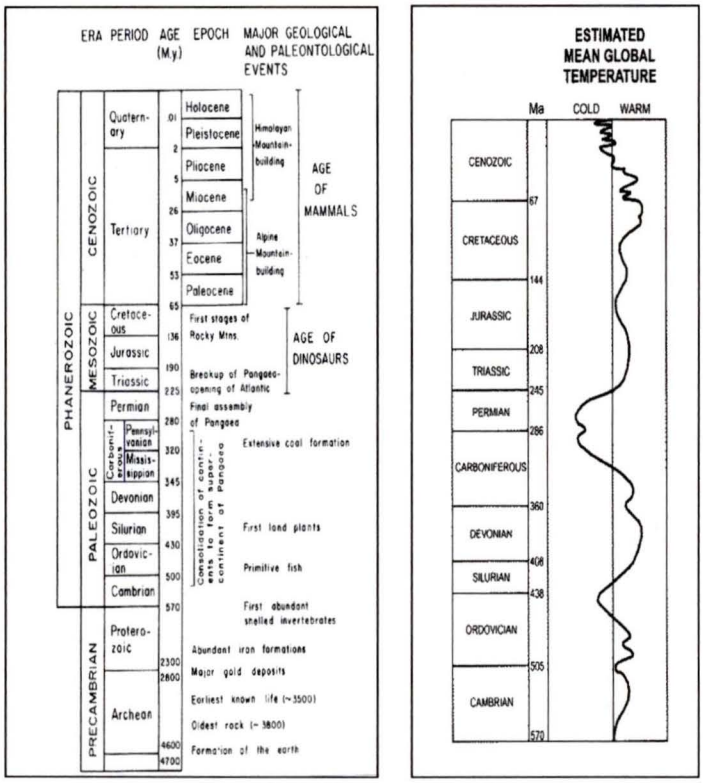

Figure 1.1: **Left: Geological time scale from Crowley and North (1991); Right: Generalized temperature history of the Earth from Frakes et al. (1992).**

1.2 Paleoclimate

1.2.1 Quaternary climate

At the end of the Cretaceous, the opening of the Pangea brought most of the continental masses in the Northern Hemisphere and provided the modern latitudinal distribution of the continents and the oceans. Consequently, the climate kept cooling through the Cenozoic and eventually geological features as well as orbital parameters became favorable for the development of continental ice sheets. The ice sheet over Antarctica appeared 15 My ago in the Miocene at the opening of the Drake passage, whereas the first Northern Hemisphere

ice sheet formed only 2.54 My ago. 1.2 My ago, in the middle Pleistocene, the dominant ice volume variation cycle shifted from 41 ky to 100 ky, without any drastic changes in orbital forcing (Imbrie et al. 1992). This shift is recorded in both polar ice isotopic profiles, and deep marine sediments (Clark et al. 1999), leading to the conclusion that transitions in ice sheet cyclicity drive changes in the global climate system.

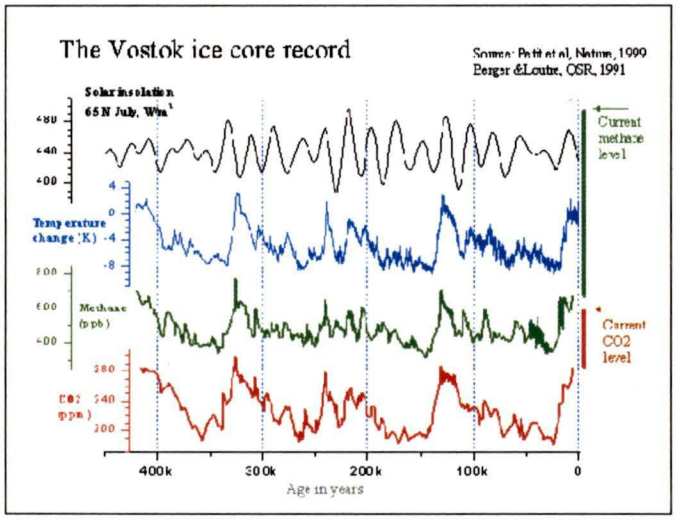

Figure 1.2: **Vostok ice core record (Petit et al. 1999) correlated with July insolation at 65°N from Berger and Loutre (1991).**

A recent ice core of 3 623 m drilled in Vostok, Antarctica, has provided valuable informations on the recent glacial-interglacial cycles, including local temperatures, aerosols fluxes and trace gases concentrations (Petit et al. 1999). The chronology based on physics (not tuned with orbital parameters) and correlated with Northern Hemisphere (NH) summer insolation variations. It reveals an obvious 100 ky periodicity.

The data-set spans four glacial-interglatial cycles (fig. 1.2). Each cycle exhibits the same pattern: a long and progressive glaciation ending when the NH summer insolation is minimum with a rapid termination. The amplitude of surface temperature changes over the cycles is about 12°C. The increases in Vostok's temperature are in phase with increases of NH summer insolation and of greenhouse gases, while the dust and aerosol concentrations decrease. During glacial periods, however, the high concentration of dust and aerosol suggests a more arid and more windy climate in the high southern latitudes, in agreement with the loess deposits observed in Patagonia. The intensification of winds is caused by a

steeper meridional temperature gradient. Sea ice extent increased toward lower latitudes (CLIMAP Project. 1981) and the deep oceanic circulation was reduced (Boyle and Keigwin 1987).

These results suggest that the same sequence of climate forcing operated during each termination: the initiation of the warming occured by increase in NH summer insolation and is followed by two strong amplifiers, greenhouse gases acting first, then deglaciation and ice-albedo feedback. A short interglacial with today's conditions then prevails for a few thousand years before the climate once again falls into the next glaciation when the NH summer insolation decreased. The variability of 100ky corresponds to that of the orbital parameters. But understanding how the climate respond to this initial forcing is still an important issue in paleoclimatoly (Petit et al. 1999).

Each interglacial stage differs slightly in evolution and duration; however the present one, the Holocene, is undoubtly the longest (11,500 yrs) observed over the last 420,000 years. Moreover, present day concentrations of CO_2 and CH_4 reach unprecedented values: respectively 370 *ppm* and 1760 *ppb* against maxima of 285 *ppm* and 760 *ppb* during the late Pleistocene (Quaternary glacial cycles). This shows that the climate system has been brought out of its natural bounds. It is however necessary to understand how natural climate variability operates before we can try to predict future reactions to anthropogenic perturbations.

1.2.2 Millennial scale climate change - Bond cycles

Marine sediment and ice core isotope profiles show long 100 ky oscillations (driven by orbital forcing) in which shorter millennial variations are embedded. The Earth's climate has varied continuously at time scale at least as short as thousand years (fig.1.2).
Dansgaard et al. (1993) present the $\delta^{18}O$ profile from an ice core drilled at Summit, central Greenland, and spanning the last 250 ky. In polar ice, the $\delta^{18}O$ mainly records the temperature of precipitation. The profile shows large, abrupt variations over time suggesting that the climate in the North Atlantic region "is able to reorganize itself rapidly, perhaps in a few decades". The abrupt $\delta^{18}O$ shift reflects rapid change in temperature, amounting to 6 to 8 °C (Dansgaard et al. 1984) over Greenland and the North Atlantic region. These shifts are known as the Dansgaard-Oeschger events (D-O) and occur with a cyclicity of about 1500 years.

Heinrich (1988) and then Broecker et al. (1992) noticed 6 layers with a high concentration of lithic debris in a North Atlantic marine core spanning the last glaciation. They attributed them to 6 armadas of icebergs coming from the Laurentide ice sheet and melting in the North

Atlantic. Broecker et al. (1992) claimed that the fresh water from the iceberg melting could have disrupted deep water formation, and hence the thermohaline circulation, exerting a strong control on the North Atlantic climate.

The link between Heinrich events and temperature changes over Greenland leads to the idea that fresh water released by the iceberg melting disrupts North Atlantic Deep Water (NADW) formation, permitting a switch between glacial and inter-glacial modes.

Ice cores recording air temperature, and marine cores recording surface salinity henceice discharge, reveal interglacial periods followed by a serie of D-O oscillations. From one oscillation to the next, the climate is cooling and the ice sheet is growing until is reaches a maximum thickness for which the high pressure at its base induces melting and surging of the ice-sheet into the ocean. This represent an Heinrich event. The ice sheet melting accompanied with ice-albedo and greenhouse feedbacks, finally triggers a rapid warming bringing back the system to the next interglacial. This succession of a cold Heinrich event followed by rapid warmings and progressive cooling with D-O oscillations, represents a Bond cycle and occurs on a time scale of 7-10 ky (fig. 1.3) (Alley et al. 1999).

Imprints of the Heinrich events and D-O oscillations are seen throughout the world in many different climate proxies like CH_4 trapped in Greenland ice, pollen in American lakes, lakes level in Africa, maximum glacier extension in the Andes and New-Zealand Alps and $\delta^{18}O$ from Antarctica. However, their signatures are attenuated when moving away from the North Atlantic, suggesting that they are initiated in this region and transmitted over the Earth by oceanic and/or atmospheric processes. The D-O oscillations correspond to significant equatorward expansion of the polar front in North Atlantic high latitudes, while the mid and low latitudes remain almost constant (Crowley 1981).

Each of the six Heinrich events starts when the ice caps throughout the world reach their maxima (Broecker and Denton 1990), and are followed by a rapid retreat of glaciers and sudden warming in a period of a few decades. According to Broecker (1991) after the surge of the ice sheet in the North Atlantic ocean, the iceberg armada's melting produced a fresh surface layer responsible for the "shut off" of the thermohaline circulation, which in turn considerably reduces the heat release to the atmosphere. This mechanism had been successfully reproduced by model simulations conducted with the UVic Earth system climate model (Schmittner et al. 2002a, Meissner and Gerdes 2000).

1.2.3 Climate reconstruction of the last glacial cycle (150 kbp)

The purpose of this thesis is to study the evolution of NADW formation, the driving force behind the thermohaline circulation, through the last glacial cycle. Therefore, after an

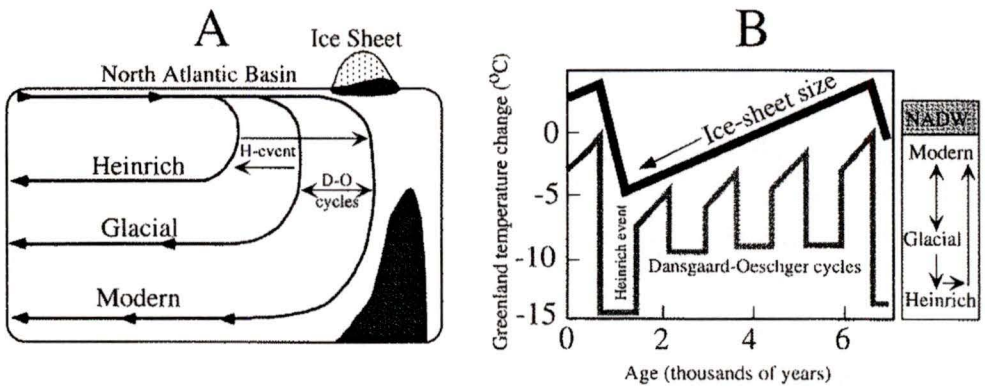

Figure 1.3: **Schematic representation of the Bond Cycle from Alley et al. (1999).**

overview of the general Quaternary climate, the last glacial cycle will be described in more detail and represented on figure 1.4. Around 150 kbp the strong glacial stage shifted abruptly to the last interglacial from 130 kbp to 115 kbp. Afterward, temperatures started to decrease unsteadily, undergoing a succesion of Bond cycles, to reach minimum values at the last glacial maximum around 21 kbp, and eventually to increase again, starting the present interglacial.

Penultimate interglacial (130 - 115 kbp)

At about 130 kbp, $\delta^{18}O$ records indicate a rapid and intense deglaciation with more ice removal than for the most recent one ($\sim$14 kbp ago). The Eemian is associated with the minimum ice volume, as defined by the marine isotopes substage 5e, and lasted from 127 kbp to 118 kbp (Adkins et al. 1997). During the interglacial maximum around 125 kbp, some coral reef studies indicate a sea level 6 metres higher than at present (Ku et al. 1974). Geochemical studies of bottom-dwelling organisms provide intriguing indications of differences between the present and the last interglacial. δ^{13}C data from the North Atlantic being lighter than currently, can be interpreted as greater Antarctic Bottom Water (AABW) production and/or less NADW production (Duplessy et al. 1988).

Temperature estimates are available for a few land regions. Records mainly from western Europe suggest temperatures at least 1-3°C warmer than during the present interglacial (de Vernal et al. 1986), and temperatures were 2-3°C warmer than at present in East Antarctica (Petit et al. 1999). On the other hand the SST reconstruction for 120 kbp (CLIMAP Project. 1984) show temperatures generally similar to the present ocean. Summer

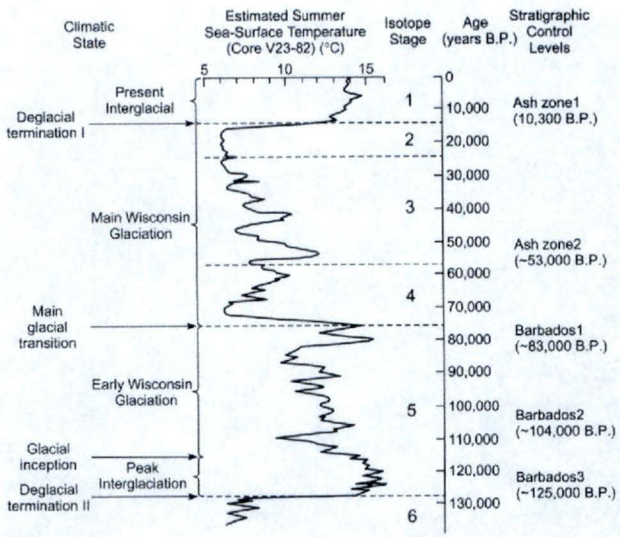

Figure 1.4: **Summer sea surface reconstructions for the North Atlantic Ocean based on faraminifera assemblage paleotemperature estimates, using core V23-32 from 53°N 22° W (Sancetta et al. 1973).**

precipitation in African and east Asian sectors of the monsoon was apparently greater than today (Liu et al. 1985, Petit-Maire 1986). Model results from Prell and Kutzbach (1987) also agree and relate an increase in temperatures with an increase in the monsoon. This pattern of higher temperatures over land and displacement of low pressure system over the North Atlantic results in an intensification of winds over the central region of the North Atlantic. Because of the conservation of the angular momentum, acceleration of winds should result in a shrinkage of the North Atlantic gyre, intensifying the Gulf Stream and the equatorward transport along the eastern margin of the North Atlantic. Both geological data and model results agree with this assumption (Crowley 1981, Prell and Kutzbach 1987).

Glacial onset (115 - 75 kbp)

Following the interglacial, the onset of glaciation is marked by two major stages of ice volume growth, at 115 kbp and 75 kbp. These features are visible in the Greenland and Vostok (fig. 1.2) ice cores records (Dansgaard et al. 1993, Petit et al. 1999) by rapid temperature drops.

The first phase, from 115 kbp to 75 kbp, includes two cold and two warm periods during which the ice volume grew and decayed with an overall increase. While ice was growing, geological records suggest an extreme aridity in north West-Africa associated with

weak Atlantic trade winds (Pokras and Mix 1985). It has also been proposed by Labeyrie et al. (1987) that deep water temperatures decreased by 1-2°C implying that the formation of deep water is still active but colder than in the interglacial period. Finally, the CO_2 concentration decreased more or less in phase with the temperature. The main glacial stage was reached during the second phase of the glaciation, from 70 kbp to 14 kbp.

The variations of ice volume and temperature during this period follow the pattern of Bond cycles closed by Heinrich envents (every ~10 ky or so). These cycles induce sea level variations of 30-40 m (Crowley 1981).

Last Glacial Maximum, LGM (22 - 14 kbp)

The glacial maximum was reached at ~21 kbp (H2) and lasted until ~14 kbp. At that time the Laurentide ice sheet represented half of the total ice on the globe. Its thickness, as well as the Fennoscandian's, was about 3000 m (CLIMAP Project. 1981), causing a lithosphere depression of $\sim$ 700 m. The sea level was 121 ± 5 m below the present level (Fairbanks 1989), which strongly influenced the climate by affecting the carbon cycle and surface albedo. The winter snow cover was also twice as large as today (Crowley 1981).

The mean annual temperature in mid-latitudes, around the Laurentide and Fennoscandian ice sheets, is generally estimated at 10°C lower than today (CLIMAP Project. 1981); in the tropics it is estimated to have been 4-5°C lower than today. The climate was generally more arid, especially in the tropics. Exceptions were northwestern Africa, the Middle East, southern Australia and southern South America, where the equatorward displacement of the mid-latitude low pressure system placed them under the storm track (Crowley 1981). The climate was also more windy; small but various proxy data sets consistently indicate that global surface wind speeds may have increased anywhere from 20 to 50 %. Such large changes in forcing are expected to exert strong effects on the ocean circulation as well as the sea-ice formation, by increasing the ocean heat loss to the atmosphere (Crowley and North 1991). The CLIMAP Project. (1981) study updated by the alkenone proxy method (Rosell-Melé 1997) gives a representation of the paleo Sea Surface Temperature (SST). In regions affected by the migration of sea ice and the oceanic polar front, the SST decreased by 6-10°C; over the tropical oceans the decrease is only 1-2°C. On the basis of geochemical and paleoforaminiferal studies, Curry et al. (1988) suggested that the NADW production was reduced, and intermediate water production increased.

The cold period between 18 - 14.5 kbp, known as the Oldest-Dryas, leads to the last Heinrich event (H1) and is followed by a rapid warming which terminates the LGM.

Deglaciation, Bolling-Allerod (14 - 11 kbp)

The major deglaciation of the Northern Hemisphere was initiated after H1, at ~14.5 kbp. Typical of glacial terminations, the melting of the great ice sheets occured within a few thousands years, most of the ice had disappeared at 9 kbp. However, the aridity in Africa remained high until 13 kbp, which is normally characteristic of glacial periods. There seems to be some sporadic production of NADW indicating a transition state. The onset of deglaciation really occured at 13 kbp with a global warming and the northward retreat of the polar front in the North Atlantic (Crowley 1981).

Younger Dryas, YD (11 - 10 kbp)

In contrast to other deglaciations of the Northern Hemisphere, this last rapid warming was interupted by a major cold event lasting for a thousand years or so, and leaving its imprint throughout the world. The Younger Dryas (YD) has been described as an Heinrich event (H0) because of its cold climate, followed by a rapid warming. The YD's ending brings us to the Holocene present climate and its relatively long term stability.

The very sudden and cyclic variations over the late Quaternary are still not well understood, but are evidently the result of interactions between ice sheet dynamics and ocean - atmosphere circulation.

1.3 Oceanic circulation

1.3.1 Present

The global ocean, with the atmosphere, is one of the two principal actors in the climate system, in the sense that it redistributes heat from low to high latitudes by the way of oceanic currents. This general circulation consists of two interactive components: the surface circulation driven by winds and organized in large gyres within the ocean basins; and the deep circulation, driven by the water mass density gradients due to change in temperature and salinity, named for this reason the thermohaline circulation and pictured as the "conveyor belt" by Broecker (1987).

The initiation of the deep meridional circulation takes place in the North Atlantic high latitudes, where warm salty surface water from tropical regions is cooled down and hence becomes more dense and sinks to the bottom of the basin. This deep water moves southward in a Western Boundary UnderCurrent (WBUC) following the American continental margin until reaching the Antarctic Circum polar Current. From there, the mixed water is

redistributed to the upwelling zones, usually on the east side of oceanic basins and in the equatorial divergence zones. Coming back to the surface, the water eventually returns to the North Atlantic, continuing the loop.

The northern North Atlantic is an important location as it is a place where the surface water is converted into deep water. The NADW comes from two different sources:
1/ Labrador Sea Water (LSW), formed by winter convection in the Labrador Sea (LS). The LSW, sometimes known as "Upper NADW", is the warmest and shallowest part of the NADW, moving southward with the WBUC above the "lower NADW" (McCartney and Curry 2002).
2/ The "lower NADW" (LNADW) comes from the overflow water (Worthington 1970). Intermediate Nordic Sea water entering the North Atlantlic in the Irminger basin, flows above the shallow sills. Two types of overflow water are distinguished:

- On the western part of the Irminger basin is the Denmark Strait Overflow Water (DSOW), coming from Denmark Strait, 600 m deep. Its temperature and salinity are usually about 1°C and 34.9 psu.

- On the eastern part is water coming from the Iceland-Scotland Ridge, 450 m deep, and the Faroe channel, 850 m deep. This water mass is a bit saltier than the DSOW as it mixes with the thermocline when passing above the ridge.

The overflow water sinks to the bottom of the basin and moves south-westward. It follows the basin boundaries, along Greenland and around LS, hence entraining the LSW, until it reaches the Antarctic Bottom Water (AABW) around 40°N, with which it mixes, to form the lower NADW. These processes are sketched in figure 1.5.

The motion of warm surface water moving northward and cold deep water moving southward represents the meridional overturning. It is generated by the large scale meridional density gradient between the dense surface water from the arctic and the light surface water originating from the south Atlantic basin.

The meridional overturning represents a latitudinal-vertical volumic transport zonally integrated between two fixed meridional boundaries, on which the zonal velocity is assumed to vanish (shore lines). It is expressed in Sverdrup ($10^6 \mathrm{m}^3\ \mathrm{s}^{-1}$). The estimation of the North Atlantic meridional overturning cell is one of the climate models objectives. Estimations from shipboard data analyses are hard but consistent. Based on oceanographic sections and current measurements at 24°N in the Atlantic, it has been estimated that 17±4 Sv thermocline water flows northward, 20±5 Sv North Atlantic Deep Water (NADW) flows southward below it (as a deep western boundary undercurrent), and 3±3 Antarctic Bottom

Water (AABW) flows northward further below the NADW (Roemmich and Wunsch 1985). An overturning maximum value in the North Atlantic has been estimated at 18 Sv by Rintoul (1991). The maximum overturning in the North Atlantic is used as a measure of the strength of the thermohaline circulation.

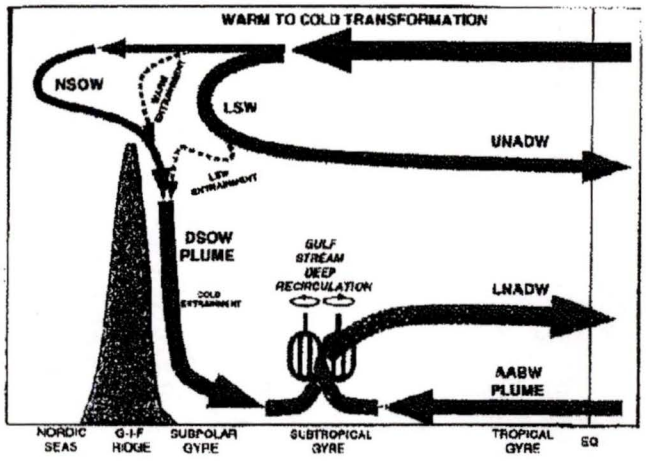

Figure 1.5: **schematic profile of meridional overturning circulation from McCartney and Curry (2002)**

1.3.2 Variations

The oceanic circulation is believed to have varied with time. The paleoclimate research community has been studying the cyclicity of late Quaternary climate, particulary millennial variability which is too short to be generated by orbital forcing. A common conclusion is a "turn on and off" of the conveyor belt (Broecker et al. 1990), leading to variations in ocean heat transport and high latitude heat release to the atmosphere. The traditional explanation to this switch, is an input of fresh water in the region of deep water convection due to ice sheet melting or surging (Broecker 1994). The mechanisms for millennial scale climate variability are based on the assumption that ice sheet - ocean - atmosphere interactions in the North Atlantic region drive the climate changes elsewhere through transmission by atmospheric dynamics, oceanic dynamics and amplifying feedbacks.

Alley et al. (1999) suggests that the North Atlantic Ocean operates in one of three distinct modes of circulation (*fig.* 1.3):

1/ The modern mode, characterised by deep water formation in the Nordic Seas and further south in the North Atlantic, is associated with a warm climate in the North Atlantic.

2/ The glacial mode, for which deep water formation in the Nordic Seas is largely stopped, but North Atlantic Intermediate Water (NAIW) formation continues farther south in the North Atlantic. The NAIW forms farther south, because of a strong northern cooling and widespread cold, dry and windy conditions associated with the stadial (cold) times of the D-O ocsillations and glacial maxima.

3/ The Heinrich mode has deep intermediate water formation greatly reduced in both locations (the previously mentioned "turn off" of the thermohaline circulation). The Heinrich mode is forced by meltwater events associated with Heinrich events that cause only small additional cooling in high northern latitudes, but greatly reduce NADW formation and subsequently trigger a rapid warming (Alley et al. 1999).

The thermohaline circulation supposedly alternates between the modern and glacial modes at the D-O oscillation rhythm. The climate is getting cooler and cooler, until it reaches a threshold and switches from the glacial to the Heinrich mode due to a surging event and rapidly goes back to the modern mode once fresh water from ice sheet calving stops, and starts anew (Schmittner et al. 2002b).

High resolution geochemical records from the North Atlantic and the Nordic seas identify significant geographic and temporal variability in surface water hydrology (T-S) and deep ocean circulation. The $\delta^{13}C$ in the ocean is a geochemical tracer of deep-ocean nutrients distribution and monitors past variations of deep water circulation. The organisms living in surface waters preferentially use light carbon, which accumulates in deep water over time by dissolution of sinking organic matter. Thus newly formed deep water has a high $\delta^{13}C$ which decreases over time (Sarnthein et al. 1994). During the LGM, $\delta^{13}C$ variations indicate an absence of NADW at the bottom, but rather NAIW filling the glacial North Atlantic to 10°S (Sarnthein et al. 1994). The $\delta^{18}O$ records from deep sea sediment indicate that the NAIW was probably convecting in the open-ocean, somewhere south of Iceland (Duplessy et al. 1996). At ~21 kbp a major change occured in the geochemical data, representing the cooling of the Oldest Dryas leading to H1. At ~14.5 kbp, $\delta^{18}O$ records from deep sea sediment suggest a widespread low salinity lid preventing the convection of intermediate water (Sarnthein et al. 1994).

Afterward, at the onset of the Bolling-Allerod warm interval, Greenland ice core $\delta^{18}O$ values increased in the North Atlantic for the rest of the deglaciation which also indicates an SST and SSS increase (Lehman and Keigwin 1992). Nutrients levels returned to their interglacial value suggesting a re-establishment of the modern deep-ocean circulation and excursions of $\delta^{18}O$ value remained relatively small during the deglaciation.

Some other records, especially those of Zanh et al. (1997) show the same pattern before

each Heinrich event, that is a weakening of NADW, low SST and SSS. Moreover Rasmussen et al. (1996) reconstructed deep water overflow from the Nordic seas with a core covering H5 to H1, and found strong outflow during the warm and transitional periods, but little or no overflow during each of the cold of D-O stadials.

The reconstruction of the late Quaternary climate, its relation with the general oceanic circulation and its variations has been built from continuous data analyses over the last few decades. Recent improvements in numerical computation have also given new opportunities to test theories by representing global climate dynamics in numerical simulations.

In the following chapters the UVic Earth system climate model is used to simulate the climate at different critical states of the last glacial cycle. In the next chapter the model, as well as the differents experiments conduted for the thesis, are described.

Chapter 2

Model and experiments

2.1 Model description

All the experiments described in this thesis have been run using the UVic Earth System Climate model. It is a coupled climate model of intermediate complexity, with a 3.6° longitude by 1.8° latitude resolution. It consists of three components: atmosphere, ocean and sea ice. The model uses spherical coordinates: the longitude is positive eastward, starting at an arbitrary point. The latitude is positive northward, zero being the equator, and the vertical coordinate increases upward with zero at the surface of the ocean. The grid is rotated in order to have the north pole in Greenland while the south pole remains in Antarctica, thereby removing the problem of grid convergence near the north pole. The model resolves the annual cycle and can simulate the climate under various radiative forcings prescribed through changes in the orbital parameters and the atmosphere CO_2 concentration. Here emphasis is on the ocean circulation model which does not use flux adjustment. As it doesn't need boundary conditions at the ocean surface, it is a good tool to simulate past or future climates with radiative forcing considerably different from today. The model, described briefly here, is fully detailed in Weaver et al. (2001).

2.1.1 Atmosphere model

The atmosphere component is a two dimensional energy-moisture balance model (EMBM) based on Fanning and Weaver (1996). The two prognostic variables are the surface air temperature (T_a) and the specific humidity (q_a). Temperature and moisture decrease with altitude, following a vertically integrated energy-moisture balance equation. Their horizontal transport is parametrised with eddy diffusion coefficients. In addition, the model parametrises a series of feedback mechanisms: ice-albedo, water vapour, rain-snow temperature threshold and melting rate.

Energy balance

The atmosphere thermodynanic energy balance equation is expressed as:

$$\rho_a H_t C_{pa} \frac{\partial T_a}{\partial t} = Q_{HT} + Q_{SSW} - Q_{OLW} + Q_{LW} + Q_{SH} + Q_{LH}^P - Q_{LH}^M \tag{2.1}$$

where ρ_a is the air density at the surface, H_t is a constant scale height for pressure and $C_{pa} = 1004$ J kg^{-1} K^{-1} is the specific heat of air at constant pressure.
On the right hand side, Q_{HT} is the net horizontal heat transport and Q_{SSW} the shortwave radiation absorbed by the atmosphere. Q_{OLW} is the outgoing longwave radiation, Q_{LW} the net upward longwave radiation at the surface, Q_{SH} the surface sensible heat flux, Q_{LH}^P the latent heat release associated with precipitation, and Q_{LH}^M the latent heat consumption associated with snow melting over land.

The incoming solar radiation at the top of the atmosphere depends on the orbital parameters. Only part of it is absorbed by the earth system due to the latitudinally dependant planetary albedo α. To consider the ice and snow feedback, α increases by $\Delta\alpha$ varying from 0 to 0.18 depending on the ice and snow thickness. 30% of the short wave entering the system is absorbed by the atmosphere and 70% is absorbed by the surface. The water vapour feedback and radiative forcing associated with green house gases are included in the Q_{OLW} which depends on the atmospheric water vapour and CO_2 concentrations as well as the surface air temperature. T_a also varies according to the topography, with a lapse rate of 6.5°C km^{-1}.

Moisture balance

As with energy, the atmospheric moisture content is vertically integrated. At the surface, the balance equation consists of two terms: the net horizontal moisture flux, parametrised by latitude dependent eddy diffusion coefficients, and the net vertical moisture flux, where evaporation and sublimation are sources, and precipitation is a sink. Precipitation occurs when the specific humidity exceeds 85%. Precipitation falls as rain as long as the temperature is greater than -5°C, then it becomes snow. Once the rain reaches the land surface, it is immediately transferred to the ocean (runoff) via one of the 33 river basins, *c.f.* map in Weaver et al. (2001). When snow falls on the land surface it can accumulate to a maximum thickness of 10 metres, after which the excess melts and returns instantaneously to the ocean. The snow starts to melt when the surface temperature exceeds -5°C, following a temperature dependent rate. This low temperature compensates the fact that there is no diurnal cycle.

2.1.2 Ocean model

The ocean component of the coupled model is the three dimensional Modular Ocean Model version 2 (MOM2) (Pacanowski 1996). It has 19 vertical levels. The oceanic flows, follow fundamental fluid mechanics laws and can be defined with a system of equations including 7 variables: u, v, w being respectively the zonal, meridional and vertical velocities, the potential temperature θ, the salinity S, the pressure p, and the density ρ.

To resolve the oceanic general circulation, the primitive equations use a few approximations.

1- The hydrostatic approximation, neglecting the advection and Coriolis terms in the vertical momentum equation. This is possible because of the large horizontal dimensions (4000 km) compared to the vertical (4 km).

2- The rigid lid, giving a zero vertical velocity at the surface and hence eliminating the external gravity waves propagating at the ocean surface.

3- The Boussinesq approximation, evaluating small density variations around a reference value, $\rho_o = 1035$ kg.m^{-3}, except for buoyancy terms.

The vertical convective processes are then parametrised using the explicit Rahmstorf (1993) convection scheme. The tracers (θ, S) at two consecutive levels are mixed explicitly when they are statically unstable, *i.e.* when the density of the upper level is greater than that at the lower level. The scheme, starting from the surface, is repeated to the next downward level until a static equilibrium is reached.

At the surface, the ocean is forced by the energy and moisture fluxes predicted by the atmosphere model, as well as, by a present day monthly varying surface wind field. In conditions different from today's, this wind field is modified by a feedback, using the surface air temperature field to adjust the present monthly winds into corrected winds. The sea ice model adds more constraints at the ocean surface.

2.1.3 Sea ice model

The sea ice model is a 2 dimensional thermodynamic-dynamic model, made of three components:

1- The sea ice thickness and distribution model (Hibler 1979). It calculates the net growth of ice and the compacness (the fraction of ice in a grid cell).

2- The thermodynamics is an equilibrium ice-snow system model (Parkinson and Washington 1979, Semtner 1976). Because ice and snow are assumed to have no heat capacity, the surface temperature is in equilibrium with external forcing. The model calculates the

growth rate of ice depending on the heat flux. This varies depending on wether the surface is open water, ice covered, or ice and snow covered. When the heat flux is in deficit the ice grows, and when it is excessive the ice melts. When there is formation or melting of ice, the surface salinity is also affected by parametrised brine rejection and runoff.
3- The dynamics is an elastic-viscous plastic model by Hunke and Dukowicz (1997).

2.2 Experiments and model forcing

In the following chapters, different model integrations are compared with proxy data reconstructions. Each experiment defined in Table 2.1, is run for 2000 years with perpetual seasonal forcing, in order to reach an equilibrium. The experiments provide an annual mean output as well as monthly means in order to resolve seasonal variations.

The two varying forcings given to the model are the orbital parameters determined by the year at which the model is running and the atmospheric CO_2 concentration (table 2.1). To define the insolation at the top of the atmosphere, the model uses an orbital configuration in calendar years, from Berger (1978). The insolation at the top of the atmosphere are plotted on figure 2.1**a** using data provided by Berger and Loutre (1991).

The atmospheric CO_2 concentrations used in the model come from Antarctica ice cores, namely Vostok (Barnola et al. 1987), Taylor Dome (Indermühle et al. 1999) and Dome C (Monnin et al. 2001), and is plotted on figure 2.1**b**.

runs	*125K*	*lgm*	*12K*	*6K*	*PI*	*PD*	*gw6*	*gw9*	*gw12*
year	125 kbp	21 kbp	12 kbp	6 kbp	1999	1999	1999	1999	1999
CO_2 *ppm*	280	200	243	270	280	350	600	900	1200

***Table 2.1:* model experiments**

125K stands for the Eemian integration at 125 kbp, *lgm* for Last Glacial Maximum integration at 21 kbp; *12K* and *6K* stand respectively for the simulations run at 12 and 6 kilo years before present. *PI* and *PD* are the integrations at pre-industrial and present times. *gw6*, *gw9*, *gw12* are the global warming experiments with present orbital forcing and with atmospheric CO_2 concentrations of respectively 600, 900 and 1200 *ppm*.

In addition to the perpetual forcing, three transient experiments have been pursued. Two represent integrations from the present day to 2100 with CO_2 increasing at rates of 1% and 2% per year, while the other integration covers pre-industrial days to 2100. Thereafter these integrations will be respectively called $1PC$, $2PC$ and GHG. These experiments use constant present days orbital forcing.

In the next chapter, the occurance of convective processes in the North Atlantic in the runs *125K* and *lgm*, representing the two extreme climate states of the last glacial cycle, is compared with proxy data and analysed.

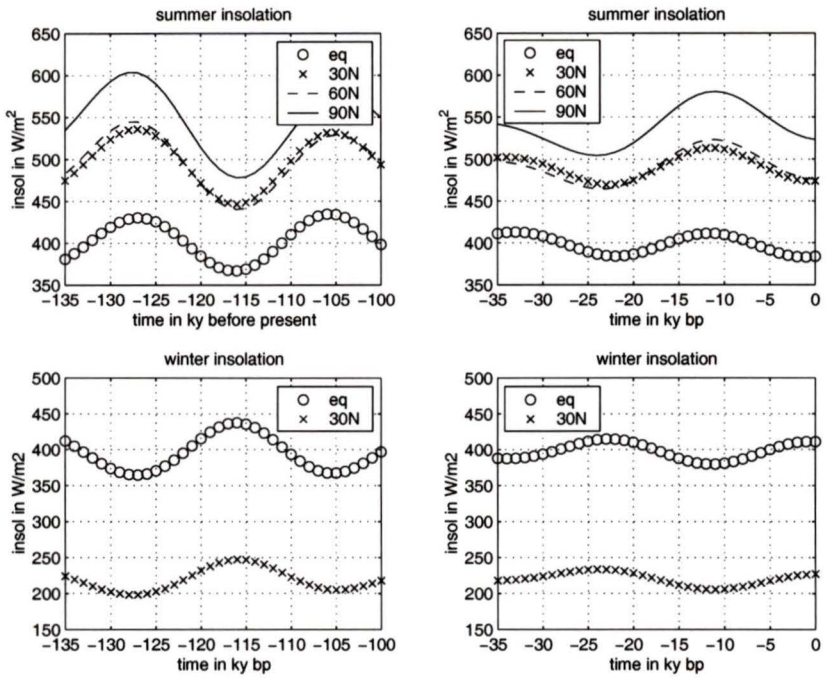

a solar forcing

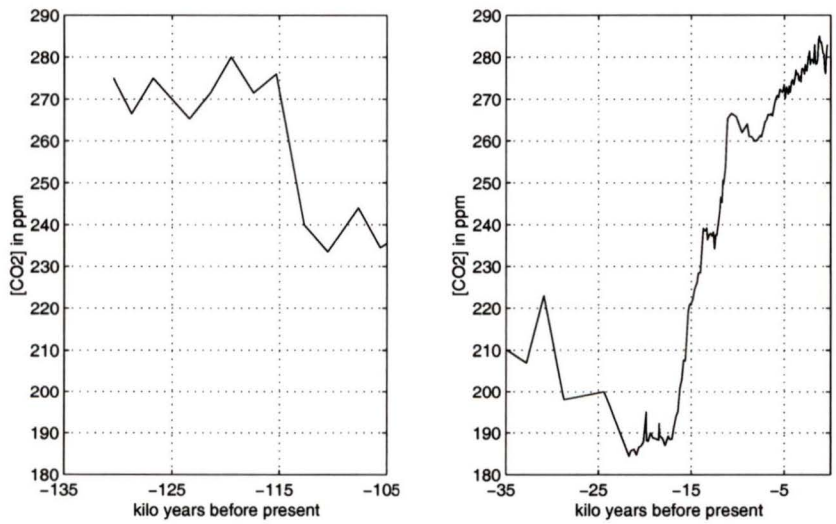

b CO_2 forcing

Figure 2.1: **Model forcing: a)Insolation at the top of the atmosphere from Berger and Loutre (1991). b)Atmospheric CO_2 concentration**

Chapter 3

Comparison: Proxy reconstruction - Model output

3.1 Introduction

In the present climate, the formation of NADW is of particular importance as it regulates the northward heat transport through the North Atlantic and has repercussions for the global climate. The deep water mainly comes from the Nordic Seas, overflowing the shallow Iceland-Scotland ridge, and entering the North Atlantic at intermediate depth. This overflow water sinks and proceeds south-westward in the boundary undercurrent, hence entraining the cold and fresh Labrador Sea Water (LSW) to form the NADW. The NADW exits the Labrador Sea (LS) at more than 2000 m via the Western Boundary Undercurrent (WBUC). The LSW is seasonally renewed by winter convection. In the winter, the relatively warm and salty the North Atlantic Drift surface water is cooled down. The LS surface becomes cold and salty, hence densier than undelying water. This unstable vertical density gradient generates a temperature and salinity vertical mixing between surface and underlying water called convection. The water column in the north-western North Atlantic can accordingly be divided into 3 water masses. The NADW below 2000 m, the LSW (Intermediate Water) resulting from convection, and the surface water. The surface layer is highly susceptible to seasonal variations, as well as longitudinal density gradients (de Vernal et al. 2002). Close to the coast, the water remains fresh and cold, leading to a strong stratification. On the other hand the offshore area is supplied with saltier and warmer water coming from the North Atlantic Drift via the Irminger current. Through winter cooling this water becomes dense and initiates deep convection.

A modelling study predicts a possible cessation of the LSW formation due to global warming (Wood et al. 1999). To investigate this possibility, studies of warm periods in the past are essential as they provide an analogue to a future greenhouse scenario. The modern warm period, the Holocene, has been stable for the last 11500 years (Petit et al. 1999). Not much is known about other interglacial periods. The last one, the Eemian, extending

from about 127 to 118 kbp (Adkins et al. 1997), is believed to have been a relatively stable period with abrupt beginning and ending due to changes in deep water flow over less than 400 years. Some studies suggest it was warmer than today by 2°C (White 1993), while some others claim that the North Atlantic sea surface temperatures were similar to the present (CLIMAP Project. 1984).

The aim of the thesis is to compare output from the UVic Earth system climate model with two paleo-reconstructions based on sedimentology and isotopes measurements from sediment cores in the north-western North Atlantic. The studies focused on reconstructing water masses properties and deep water formation in the Labrador Sea over extreme climate conditions prevailing through the last glacial cycle. First the warm Eemian, studied by Hillaire-Marcel et al. (2001), second the cold LGM studied by de Vernal et al. (2002).

3.2 The Eemian, 125 kbp

3.2.1 Proxy results

Hillaire-Marcel et al. (2001) use micropaleontological data and stable isotope measurements to reconstruct vertical temperature, salinity and thus density gradients in the water column of the LS (off southwestern Greenland). The study site consists of two oceanic cores: one on the continental slope, under the WBUC high velocity core; the other deeper and farther from the coast, on the rise, beside the high velocity core. The sedimentation rate at these locations varies. A strong WBUC corresponds to high Denmark Strait Overflow Water (DSOW), producing a low sedimentation rate on the continental slope, while sediments are deposited below, on the rise. A high sedimentation rate on the rise is observed during the Holocene and the last interglacial, indicating a strong WBUC at the entrance of the LS, hence a high DSOW production rate. On the other hand, little, if any, sedimentation is observed on the rise during the glacial period, revealing a weak WBUC at the entrance of the LS, hence a weak DSOW production rate.

Their isotopic study, based on dynoflagellates for the surface water, meso- and epi-pellagic foraminifera for the seasonal pycnocline and underlying water, and finally benthic foraminifera for the bottom water, provides proxies for temperature and salinity throughout the water column. Their retranscription into potential density indicates the presence of a fresh and cold surface layer in the LS forming a light buoyant lid which inhibites winter convection in the LS during the Eemian. However, as suggested by the sedimentation rate, DSOW remains active. The stratification between the LSW and DSOW appears only at the early Holocene when the winter convection in the LS started, around 7 ^{14}C kbp,

corresponding to ~8 kbp (Stuiver and Reimer 1993). During the Eemian, Hillaire-Marcel et al. (2001) determine that the water column was composed of a single water mass with a potential density of $\sigma_\theta \simeq 27.8$, originating from the DSOW. In the warmer climate, the fresh water forming the buoyant lid is considered to come from melting of the Arctic ice sheet via Fram strait into the Greenland current (de Vernal and Hillaire-Marcel 2000) or from more precipitation over the Arctic due to an enhanced hydrological cycle (Hillaire-Marcel et al. 2001).

In the next section, this hypothesis is tested using numerical integrations of the UVic Climate Model, which allows for a representation of the climate system, and in particular of the oceanic circulation.

3.2.2 Model results

The Eemian experiment, *125K*, is run with the 125 kbp orbital parameters, a CO_2 concentration of 280 *ppm* and present day specified ice sheet, which is believed to be correct, as at the maximum ice sheet retreat around 121 kbp, some vegetation was present in southern Greenland (de Vernal et al. 1991). In the following section, *125K* is compared with the pre-industrial simulation, *PI*, which differs from *125K* only by the variation of the orbital parameters (table 2.1).

The convection in the model integrations is represented in the left column of figure 3.1 as the maximal depth of vertical mixing in metres. The top row displays the modern situation, with active convection both in the Irminger Sea and the LS. The middle row displays the Eemian, with convection occuring only in the Irminger Sea, while ceased in the LS, in agreement with the results of Hillaire-Marcel et al. (2001). The bottom row is the LGM which will be described in the next section.

The absence of LS convection during the Eemian, affects the North Atlantic meridional overturning stream function represented in the right panels of figure 3.1. Its maximum deacreases from 21.3 Sv in *PI* to 15.1 Sv in *125K*. Consequently, in *125K*, the NADW is shallower while the AABW, the shaded contours in figure 3.1, advances further north in the North Atlantic, consistent with the paleo-record by Duplessy et al. (1988). Only 9.7 Sv of the NADW crosses the equator in *125K* against 12.8 Sv in *PI*.

Figure 3.2 contains latitudinal profiles at 60°N. The profile, noted with a red line in figure 3.1, crosses from West to East: the Labrador Sea (2200 m deep, from 60 W to 50 W), the Irminger Sea (~2200 m, from 40 W to 30 W), then it becomes shallower as it progresses along the Iceland-Scotland Ridge until it reaches the coast of Europe. From top to bottom, potential temperature, salinity and potential density are displayed for the

month of February. The left column represents *125K* and the right one *PI*. In the Eemian simulation, the fresh and cold lid in the LS, found in the reconstructions of Hillaire-Marcel et al. (2001), is clearly reproduced by the model. The LS surface density ranges from 27.6 to 27.8, and $\sigma_\theta = 27.9$ in underlying water. These values fit very well with the paleoreconstruction data, where $\sigma_\theta = 27.8 \pm 0.16$ at the surface and $\sigma_\theta = 27.9 \pm 0.12$ under the pycnocline. For the Holocene, proxies estimate the density to be $\sigma_\theta = 27.94 \pm 0.02$ along the entire water column, suggesting winter convection. Here again, the model results agree with the observations with potential density ranging from 27.90 to 27.94 in the LS water column in *PI*.

It needs to be stressed that the DSOW is not well represented in the model (fig. 3.1 and 3.2), which is a common flaw of oceanic GCMs with coarse resolution, because of the small scale processes involved in bottom flows and the necessity of having a deep and wide ridge to allow for an overflow out of the Arctic. Instead, convection occurs in the Irminger Sea, above the Iceland-Scotland ridge by cooling of the warm and salty North Atlantic Drift waters. Consequently, the North Atlantic Drift does not reach as far into the Nordic Seas as is observed, and hence the Nordic Seas are generally too cold and fresh in the model, leading to larger than observed sea ice extent. It can be noticed that the Irminger Sea convection water is colder and fresher in the Eemian run than in *PI*. This convection feeds the deep current becoming later the WBUC, which is visible in the horizontal velocity field at 1000 m (not shown here). The velocities remain similar along the Greenland slope for *125K* and *PI*, but are weaker in *125K* when exiting the LS by the WBUC because of the absence of convection in the LS. In *PI* the LS convection entrains water to the bottom which strengthens the WBUC, as predicted by the paleo-reconstructions. Hillaire-Marcel et al. (2001) explain the buoyant lid in the LS as arising from an enhanced fresh water supply from the Arctic due to increase in precipitation or ice sheet melting in the warmer period.

Contradicting the common view (de Vernal et al. 1986, Petit et al. 1999, White 1993), the Eemian integration is about 1°C colder than the present day simulation (*PD*), and about the same temperature as *PI*. The global annual mean surface air and sea temperatures for the experiments are plotted in red on the left side of figure 3.3. Their values are respectively: $\mathrm{SAT}_{125K} = 13.33$°C, $\mathrm{SAT}_{PD} = 14.12$°C, $\mathrm{SAT}_{PI} = 13.04$°C and SST_{125K} =17.71°C, SST_{PD}=18.36°C, SST_{PI} =17.57°C. The mean annual differences between *125K* and *PI* over the North Atlantic region are also visible in figure 3.4 showing warmer tropics and colder high latitudes which increase the development of the seasonal sea ice (fig. 3.6).

As noted above, the absence of convection in LS in the Eemian simulation is due to a

fresh water lid which Hillaire-Marcel et al. (2001) propose originates from either ice melting or enhanced precipation in high latitudes in a warmer climate. The Eemian simulation uses the same specified ice sheet extent as *PI*, and it is not allowed to melt, so the fresh water in the simulation cannot come from this source. Figure 3.5 shows mean annual differences between *125K* and *PI* in evaporation, precipitation and downward fresh water flux at the surface of the Ocean. The difference in evaporation between the two runs is negative (*i.e* fresher in the Eemian) only at the southern tip of Greenland where there is seasonal development in sea ice(fig. 3.6). The main difference in precipitation occurs in the same region but tends to increase the SSS. The difference above the Arctic is also negligable. Finally, the difference in the net downward fresh water flux is important only where seasonal sea ice develops. The seasonal cycle, has also been examined with the conclusion that the hydrological cycle cannot explain the presence of the fresh lid in the model. These observations support the idea that the development of the fresh lid is caused primarily by the sea ice extension (fig. 3.6).

The cold Eemian temperatures, although striking, are not in disagreement with the reconstruction from Cortijo et al. (1994), who describe a short warm period of 5000 years immediately after the deglaciation (130 kbp), with sea surface conditions similar or slightly warmer than today. This was followed by a sharp cooling and freshening in the northern North Atlantic around 123 kbp, several millenia before the next glaciation (115 kbp). Considering this reconstruction, *125K* stands in the cooling trend.

Figure 3.4 represents the mean annual differences between *125K* and *PI* over North Atlantic for SAT, SST and SSS. The surface ocean and air temperatures between 30°N and 30°S are between 0 and 1°C warmer in *125K*, while SSS is 0.1 *psu* saltier in the Gulf Stream region. North of 40°N however, the SAT and SST are 0 to 3°C colder. The SSS is also fresher with the main difference of 0.6 *psu* on the west side of the basin, in the Labrador Gyre, and a slight freshening of 0.1 *psu* on the east side of the basin. Cortijo et al. (1999) describe a surface cooling and freshening at high latitudes, with a surface warming and salinification at lower latitudes during the maximum ice retreat period, agreeing with the *125K* results. Although data tend to show that the NADW export remains active during the Eemian (Yu et al. 1996, Adkins et al. 1997), they relate the high meridional gradients of temperature and salinity to a weakened thermohaline circulation. This hypothesis agrees with a thermohaline circulation activated only by the DSOW with no convection in the LS, as described by Hillaire-Marcel et al. (2001) and observed from the model results.

It has been seen that *125K* is colder than *PI* in high latitudes. Seasonal variations of SAT and SST, plotted in figure 3.3, show that the NH winter is globally 1°C colder

in the Eemian simulation than in the pre-industrial one. Moreover, figure 3.7 shows the regional differences in air and ocean surface tempreratures between *125K* and *PI* for winter and summer. The winter is clearly colder over the entire North Atlantic, with a cold cell centered on the southern tip of Greenland and expending over all the latitudes north of 40°N as well as the continents. These low temperatures during winter in high latitudes, lead to a greater sea ice extent, reaching a maximum in February and shown in figure 3.6. In *125K*, sea ice covers the entire LS, isolating the ocean from the atmosphere. In sea ice covered region, the lack of evaporation and the continental runoff cause deacresing salinity in the upper ocean layer, another consequence is an oceanic heat loss reduction. These two processes are responsible for the development of the fresh and cold buoyant lid at the suface and preventing the LS winter convection to occur. The warm salty surface water coming from the North Atlantic Drift is not drawn anymore in the LS, building up the tendency to cool and freshen the LS surface. The extended LS ice cover is then at the origin of the cold and fresh surface lid present in the model result and deduced by paleo records.

The greater sea ice extent in the LS, arises from differences in the orbital parameters between *125K* and *PI*.

	june	90N	60N	30N	eq	30S	60S	*dec*	60N	30N	eq	30S	60S	90S
$125K$		590	534	528	425	233	23		20	203	370	460	465	514
PI		523	476	474	384	212	23		24	227	411	507	509	560
$125K - PI$		+67	+58	+54	+41	+21	0		-4	-24	-41	-47	-44	-46

Table 3.1: **Insolation in W.m^{-2}**

Table 3.1 exhibits a global insolation $\sim$ 12% larger in NH summer during the Eemian, and an even larger opposite difference in December, with insolation 10% to 16% smaller in NH winter. This suggests that the global reduced NH winter insolation is the origin of the cold temperatures at high latitudes leading to the increase of the Labrador sea ice extent. The ice cover insulates the ocean from the atmosphere inducing the cessation of convection in the Labrador Sea causing the reduction of the meridional oceanic circulation. The northward heat transport to high latitudes subsequently decreases, cooling the Nordic regions even more, and is reinforced by the ice-albedo feedback. Because of the reduced meridional overturning, the surface water aquires a longer residence time in the region of precipitation excess and thus becomes fresher. This meridional temperature and salinity gradient is perpetuated in the NH summer when the Eemian insolation, far larger than in present day, completely melts the large sea ice cover. These huge seasonal variations of insolation favour a more contrasted seasonal climate than at present. Figure 3.3 shows

a colder winter and a warmer summer both by about 1°C. Moreover, figure 3.7 shows large seasonal continent-ocean temperature gradients in *125K* in accordance with data reconstructions (Crowley 1981, Prell and Kutzbach 1987). Because of their low heat capacity during the NH winter the continents are about 2°C colder in *125K* than in *PI*. The northern North Atlantic region, due to reduced heat release from the ocean, is up to 4 to 5°C colder in *125K*. In the NH summer, the continents are $\sim$ 4°C warmer in *125K*, while the northern North Atlantic, because of the low meridional oceanic circulation, remains colder despite higher insolation.

The motivation of studying the last interglacial period was to understand natural states of ocean circulation under warming conditions and ice sheet melting. It appears that at 125 kbp, the orbital parameters promoted cooler conditions at high latitudes during winters, leading to increased sea ice growth and a reduction of the thermohaline circulation. These winters were followed by warmer summers, increasing the temperature and evaporation over low latitudes while large quantities of sea ice melted at high latitudes, perpetuing the fresh and cold surface water, inhibiting the formation of deep water in the LS. From 125 kbp to 115 kbp, the insolation increases in the winter while it decreases in the summer (fig. 2.1**a**). The winter cooling and seasonal contrast are then reduced, maintaining interglacial conditions. The summer insolation decreased until it becomes too low to melt the winter sea ice and snow, driving the climate to the next glaciation onset at 115 kbp (Dansgaard et al. 1993, Petit et al. 1999).

After the glaciation onset, the climate undergoes a succession of Bond cycles slowly cooling the system which develops large continental ice sheets over Europe and North America. It reaches a maximum ice volume at 21 kbp when the summer insolation is again at minimum values (fig. 2.1**a**). In the next section, the oceanic circulation during this period is analysed.

3.3 Last Glacial Maximum, 21 kbp

3.3.1 Proxy results from de Vernal et al. (2002)

The LGM has been thoroughly studied in paleoceanography in order to examine the variations in thermohaline circulation and deep water formation under extreme climate conditions. Interpretations of proxy data from sediment cores suggest that the NADW production was reduced but not ceased (Boyle 1995), and that in counterpart, the AABW filled a larger volume of the North Atlantic basin (Duplessy et al. 1996). A set of paleo-data reconstructions is now available to prescribe SST and SSS for ocean General Circulation Models, but

discrepencies between the different data sets persist. The ocean is globally about 1 *psu* saltier, as freshwater is stored in the ice sheets on land, as well as cooler due to the colder mean LGM climate.

A study was recently conducted at the GEOTOP, based on a transfer function for dinocysts, isotope measurements on foraminifera shells, and taking into account the plankton paleo-ecology. It provides new LGM SST, SSS, and density reconstructions for the north-western North Atlantic (de Vernal et al. 2002). Two surface water masses are distinguished, both in the coldest and warmest months. On the west side, in the LS, fresh and cold water coming from ice or iceberg melting is identifed and on the east side, in the Irminger Sea, saltier water coming from the North Atlantic Drift is found. These two water masses are mixed by two cylonic gyres meeting at the boundary of the Irminger and the Labrador basins. A warmer SST than the CLIMAP reconstruction (CLIMAP Project. 1981) is found as well as the development of a strong seasonal pycnocline between surface and intermediate water. The fresh and cold surface water constitutes a buoyant lid that shuts down winter convection. An E-W gradient is also reconstructed, with seasonal contrast increasing and surface potential density decreasing westward. This E-W gradient is claimed to be the consequence of seasonal fresh water input from the Laurentide and Greenland ice sheets. The overall surface density remains low, between ~25-27, with a pycnocline at 28.8. The higher salinity and density off Europe is the result of the northward flow of North Atlantic water feeding a cyclonic gyre in the Irminger Sea. This strong stratification does not allow winter convection in the north western North Atlantic and consequently the thermohaline circulation is thought to be weak during the LGM, in agreement with other studies (Boyle 1995, Lynch-Stieglitz et al. 1999, Rutberg et al. 2000).

3.3.2 Model results: comparison with paleo-reconstructions by de Vernal et al. (2002)

The LGM integration, *lgm*, is run with a CO_2 concentration of 200 *ppm*, and a specified continental ice sheet mask from Peltier (1996), consisting of an elevated topography and a planetary albedo raised by 0.18 where ice was present. The mean ocean salinity was kept at the modern value, not accounting for the fresh water trapped in the ice sheets dropping the present sea level by a minimum of 86 m (Clark et al. 1999).

The winter convection in *lgm* is displayed figure 3.1 in the bottom left panel, and shows the absence of convection in the northern North Atlantic. The convection totally ceases in the LS while on the eastern side of the basin, convection site shifts southward from the Irminger Sea to west of western Europe, in the Bay of Biscay. This result agrees with the

idea deduced by de Vernal et al. (2002) from the proxy analyses that convection processes cannot occur north of 50°N, *i.e.* north of Ireland.

The North Atlantic meridional overturning (fig. 3.1, right column), as expected by paleo-reconstructions, does not stop, but is substantially weakened, from 21.3 Sv in the modern situation to 12 Sv at *lgm*. The core of the NADW cell shifts south from 55°N in *PI* to 45°N in *lgm*. The NADW is also more confined in the North Atlantic basin, with only 4 Sv, *i.e.* 35% of the NADW, crossing the equator, against 60% in *PI*. The water convecting to the bottom of the basin (4500 *m*) in *PI*, sinks only to 3000 *m* in *lgm*. Consequently, the meridional North Atlantic cell is shallower, with a mean depth of $\sim$ 2200 *m* against 3000 *m* in *PI*. This allows the dense AABW to fill the basin up to 60°N below 2200 *m*.

Figure 3.8 shows latitudinal profiles of temperature, salinity and density at 60°N for the coldest and warmest months. They highlight the presence of a distinct cold and fresh lid covering the entire basin width, in agreement with the paleo-reconstructions. The February profiles can be compared with the modern situation: figure 3.2, left column. At first glance, the vertical stratification of the *lgm* ocean is striking. The North Atlantic Drift in *lgm* appears as a warm cell with a core temperature of 4°C, similar to *PI*, but isolated from the atmosphere. Since the change in mean ocean salinity due to sea level lowering has not been considered, the differences in salinity and density between *lgm* and *PI* are dynamically important. In particular, the salinity of the North Atlantic Drift cell is 0.2 *psu* fresher in *lgm* because of lower evaporation in a colder climate, and leads to lighter deep water under the pycnocline.

The fresh and cold surface water in *lgm* is the consequence of sea ice cover in the winter and sea ice melting in the summer. The seasonal sea ice variation in *lgm* is presented in the top of figure 3.9 with the maximum and minimum extent in February and August. It agrees reasonably well with the paleo-reconstructions of de Vernal et al. (2002) shown in 3.10. The summer melting of the sea ice allows only a slight warming of the ocean surface, but maintains the strong stratification which prevents convection from occurring (fig. 3.8). Under the pycnocline, the water characteristics roughly agree with de Vernal et al. (2002), showing warm and salty water on the east side of the basin originating from the North Atlantic Drift, and colder and fresher water on the west side, due to the adjacent ice sheet.

However, some differences remain between *lgm* and the reconstructions by de Vernal et al. (2002). The profile, crossing the North Atlantic from the LS to western Europe (fig. 3.8) can be compared with the figure 6 in de Vernal et al. (2002), where summer SST is predicted to increase from 2 to 12 °C when moving from the Labrador coast to the Irminger Sea. In *lgm* the temperatures are substantially colder with a maximum summer

surface temperature of 2.5°C. The summer SSS in the paleo-reconstruction ranges from 31 to 33 *psu* and increases eastward. In order to be compared with paleo-reconstructionss, 0.8 *psu* have to be added to the *lgm* salinity field (Schmittner et al. 2002a), to account for a sea level lowering of 86 *m*, which is on the lower side of current estimates (Clark et al. 1999). The summer SSS in *lgm* has a minimum of 32.8 *psu* in the Irminger Sea and a maximum of 35.3 *psu* off the Labrador coast. This makes the *lgm* simulation saltier than the reconstruction. Moreover, the reconstruction predicts saltier water in the Irminger basin coming from the North Atlantic Drift and fresher water in the LS due the adjacent ice sheet. The water masses existing in two cyclonic gyres in the Labrador and Irminger basins are mixed together at the south-eastern tip of Greenland. In the *lgm* simulation, the surface velocity map (fig. 3.9) shows the presence of a cyclonic gyre in the Irminger Sea. However, contradicting the reconstruction, this gyre encloses fresh water. This fresh water comes from the sea ice edge in winter, and sea ice melting in summer. The salty North Atlantic Drift water, which makes this gyre salty according to the reconstructions, resides 200 *m* below the surface, as previously noticed in the salinity profiles (fig. 3.8). In the LS, the surface water forms a weak gyre, with a higher salinity than in the Irminger Sea, due to brine rejection coming from Baffin and Hudson bays. These observations are in contradiction with the eastward salinification mentioned by de Vernal et al. (2002).

Because of the cold and salty surface water in the *lgm* simulation compared to the paleo-reconstruction, the surface density in the model is evenly higher by about 2 units compared to the reconstruction of de Vernal et al. (2002). In spite of the low surface density, the reconstruction suggests a permanent pycnocline at 28.8. In *lgm*, the pycnocline is effectively present all year long, but is situated at 27.5, corresponding to ~28 after the correction for the salinity which is much lower than the reconstruction.

The *lgm* model simulation agrees with the paleo-reconstructions of de Vernal et al. (2002) concerning the weakening and shallowing of the North Atlantic meridional oceanic circulation and the cessation of deep water formation north of 50°N due to the perpetual presence of a fresh and cold buoyant lid. However, the E-W density gradient mentioned above is not present in the model results. The summer fresh water input revealed by the proxy reconstruction along the Labrador coast is present in the model simulations along the ice edge in Nordic Seas, but is limited in the LS (fig. 3.8). Schmittner et al. (2002a) used an LGM simulation from the UVic Earth System Climate Model, to examine the differences of the surface properties in the north-western North Atlantic between an LGM simulation and a set of paleo-reconstructions. They found that the surface water properties reconstructed by de Vernal et al. (2002) are warmer and fresher than the model output. In fact, Schmittner

et al. (2002a) found that the model surface properties obtained with an LGM simulation are in good agreement with the CLIMAP Project. (1981) SST reconstruction and SSS reconstruction from Seidov et al. (1996). Only the reconstruction of the seasonal sea ice extent by de Vernal et al. (2002), shown in figure 3.10, agreed with LGM simulations surface properties.

The variation of the thermohaline circulation, particulary the intensity of the meridional overturning stream function, influences the North Atlantic surface properties (Manabe and Stouffer 1988). Therefore the numerical simulations must be able to reproduce surface properties deduced from proxy data, to validate the change in thermohaline circulation. In the present case, although the *lgm* surface properties do not fit with the de Vernal et al. (2002) paleo-reconstructions, they are in agreement with earlier and commonly used reconstructions (CLIMAP Project. 1981, Seidov et al. 1996). The variation of the thermohaline circulation, that is the weakening and shallowing of the meridional overturning associated with a cessation of the convective processes in the northern North Atlantic and the existence of convection in the Bay of Biscay, is consistent.

In conclusion, despite the discrepancies existing in the north-western North Atlantic surface water properties between the *lgm* simulation and the paleo-reconstructions of de Vernal et al. (2002), the general circulation pattern remains consistent. The weakening of the thermohaline circulation strength from 21 to 12 Sv, the shallowing of the meridional overturning cell with a southward shift of its core, the absence of convection in the North Atlantic but formation of intermediate water southward in the Bay of Biscay, agree with de Vernal et al. (2002) as well as with other current literature (Boyle 1995).

These characteristics are typical of a glacial state of the thermohaline circulation. Hillaire-Marcel et al. (2001) suggested that the modern thermohaline circulation pattern, with fomation of upper NADW by winter convection in the LS and lower NADW from DSOW, occurs for the first time in the Holocene, around 8 kbp, after the deglaciation (14 kbp). The next chapter is devoted to test this hypothesis.

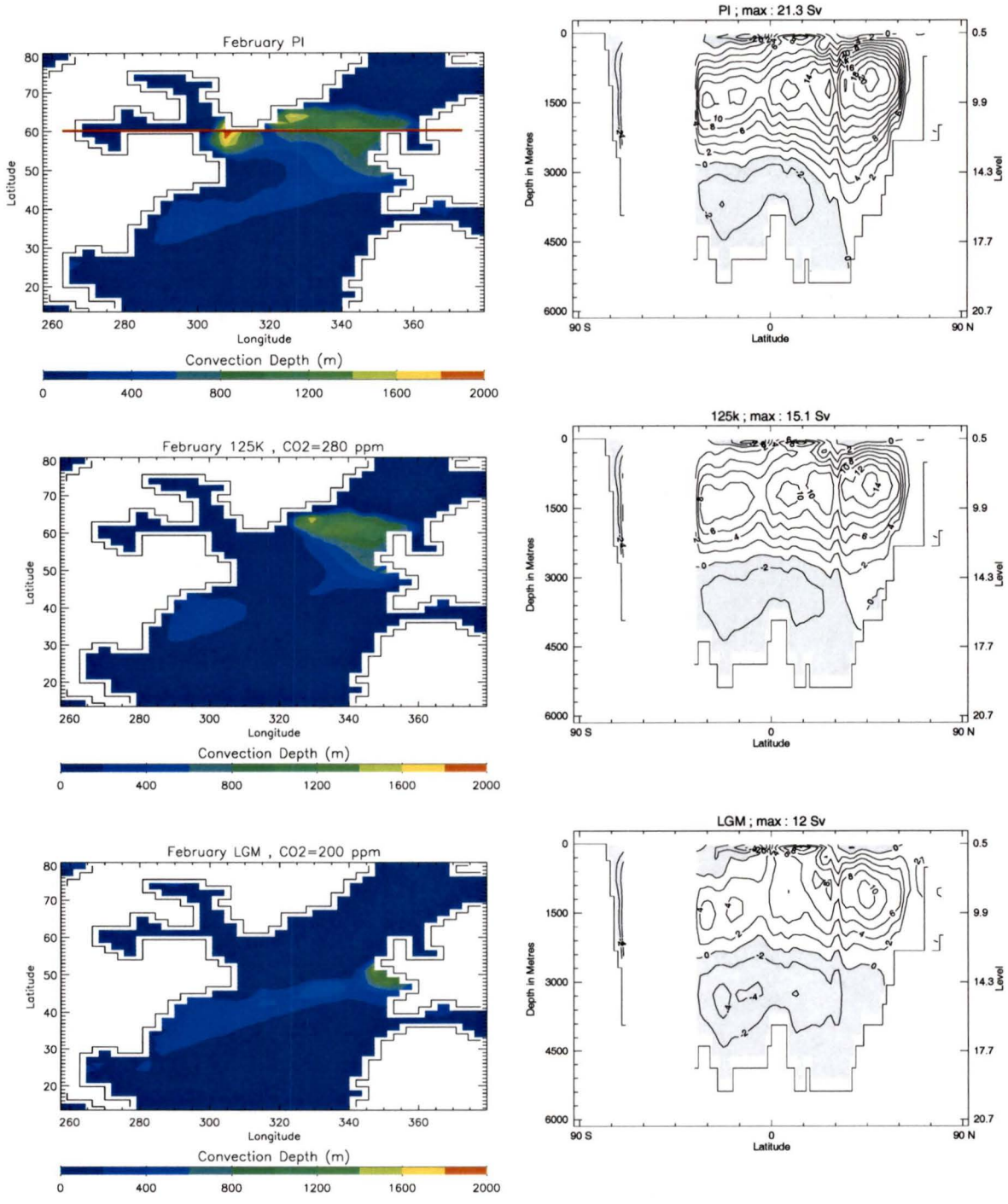

Figure 3.1: **February convection depth in m (left),mean annual North Atlantic meridional overturning stream function in Sv (right), for *PI*, *125* and *LGM*. The red line in the first pannel represents the latitudinal profile at 60°N.**

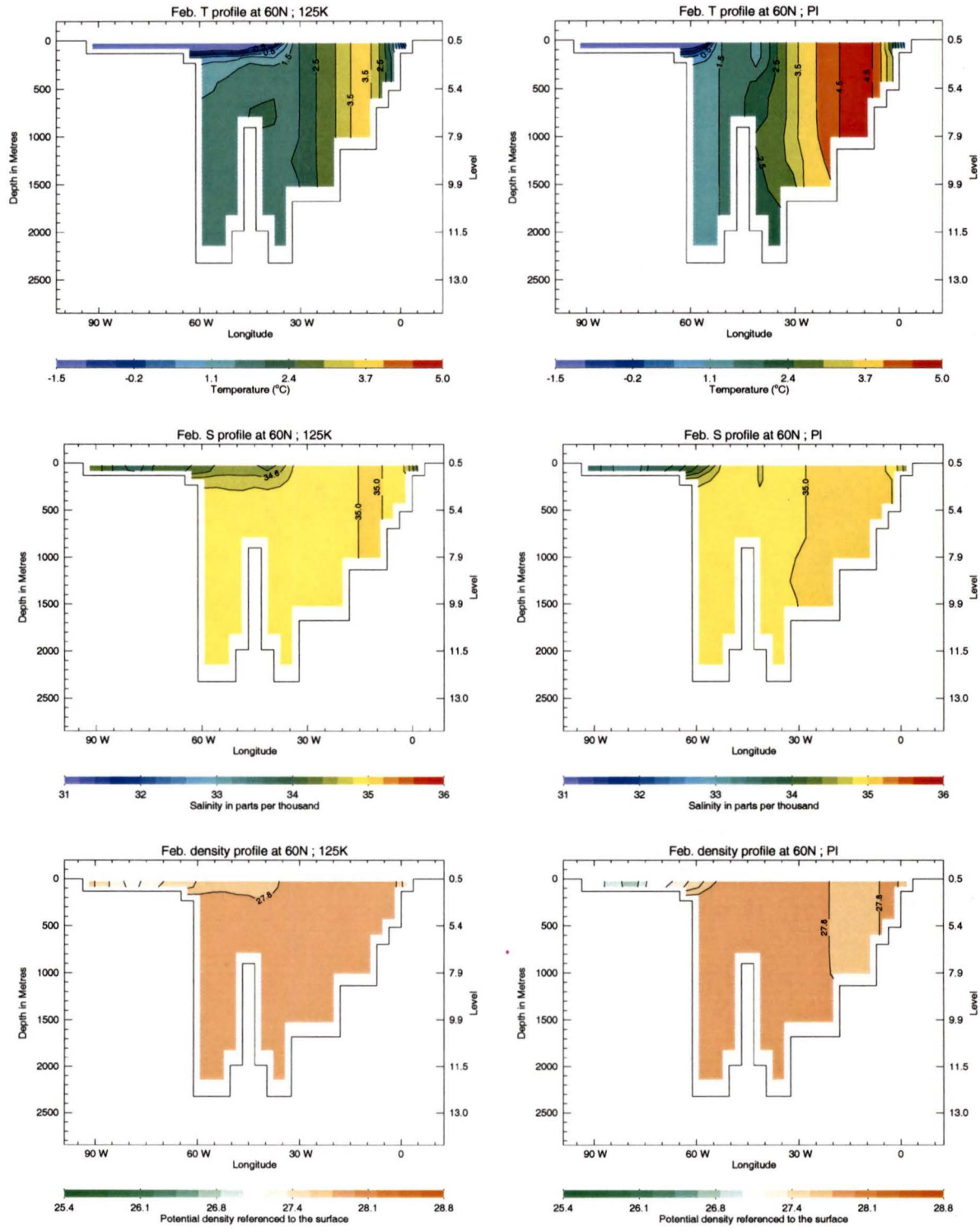

Figure 3.2: **Temperature, Salinity and Density profiles in February at 60°N across the LS, the Irminger Sea and the Iceland-Scotland Ridge. Left column: *125K*, right column: *PI*.**

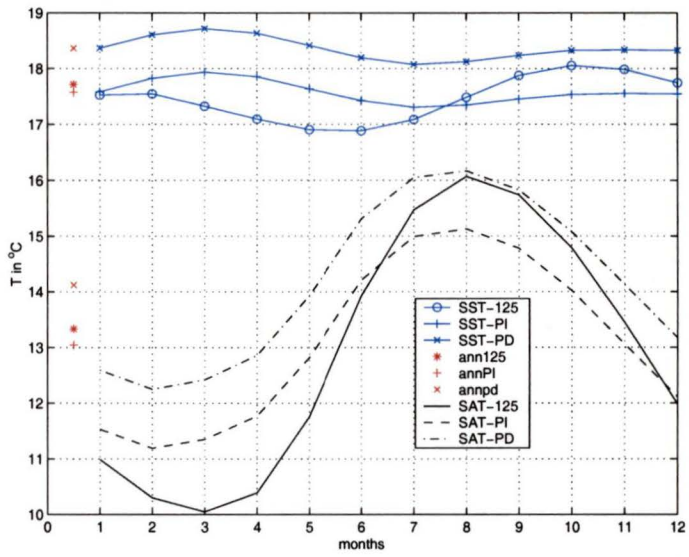

Figure 3.3: **Mean annual SST and SAT (red) plus seasonal variation of globally-averaged SST (blue) and SAT (black) for *125K*, *PI* and *PD*.**

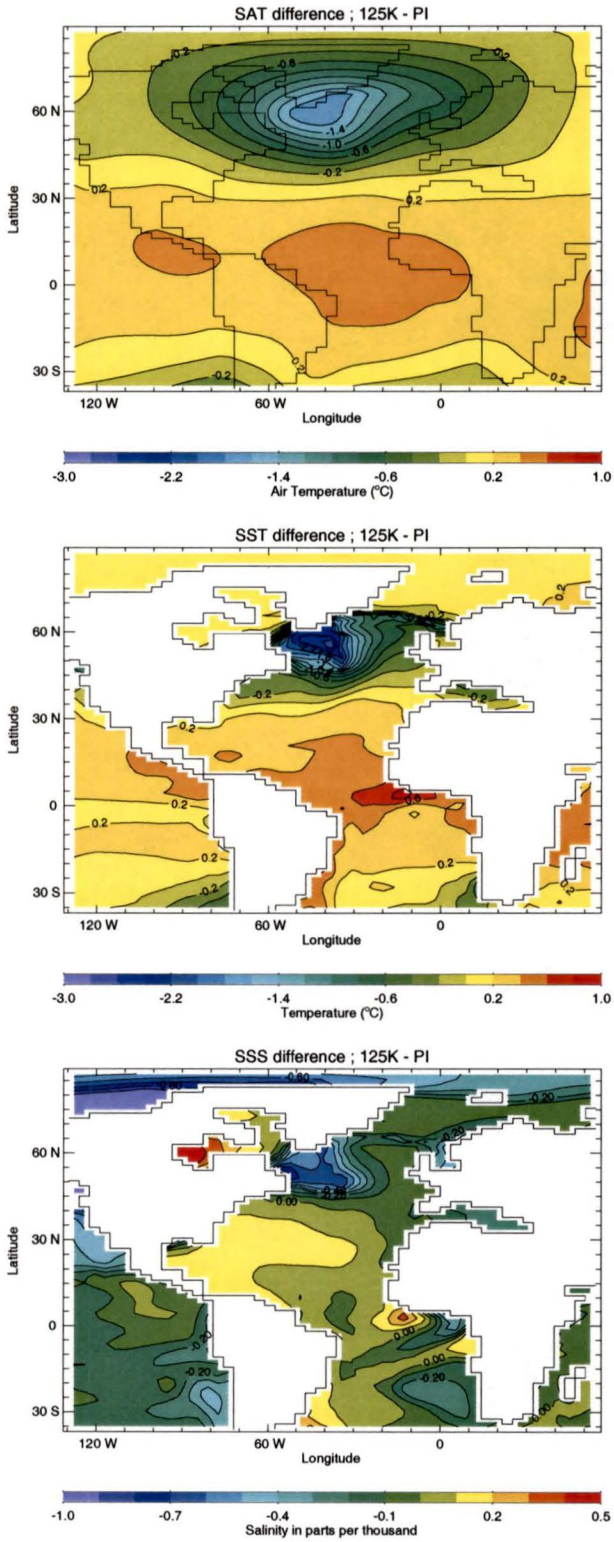

Figure 3.4: **Mean annual differences (*125K – PI*) in SAT, SST and SSS.**

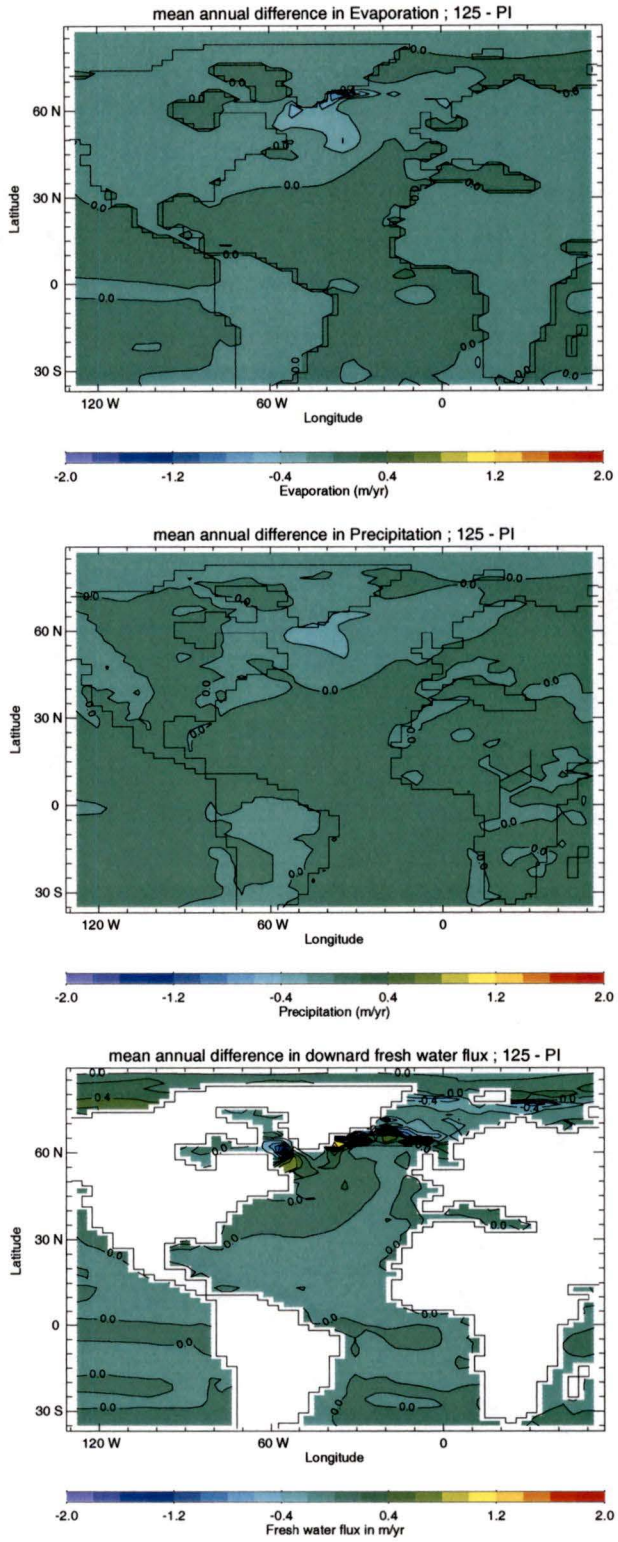

Figure 3.5: **Differences (*125K − PI*) in freshwater forcing: evaporation, precipitation and downward freshwater flux.**

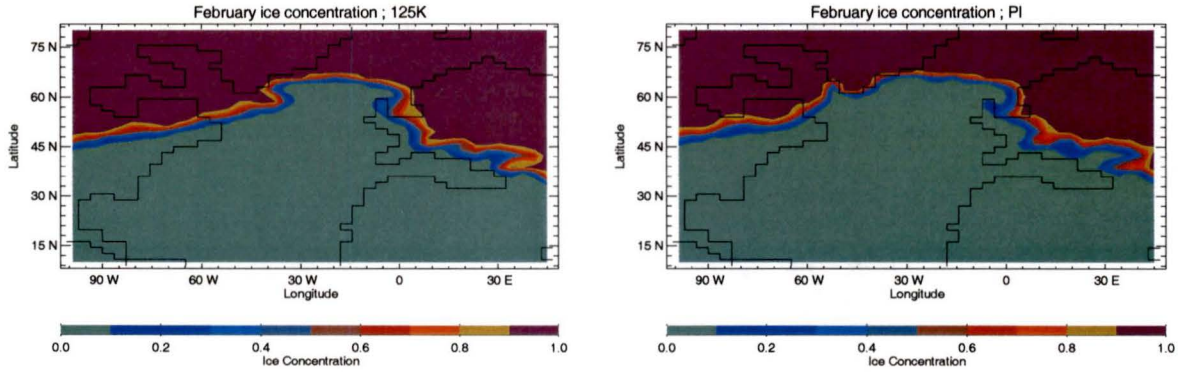

Figure 3.6: **February sea ice concentration: *125K* (left) and *PI* (right).**

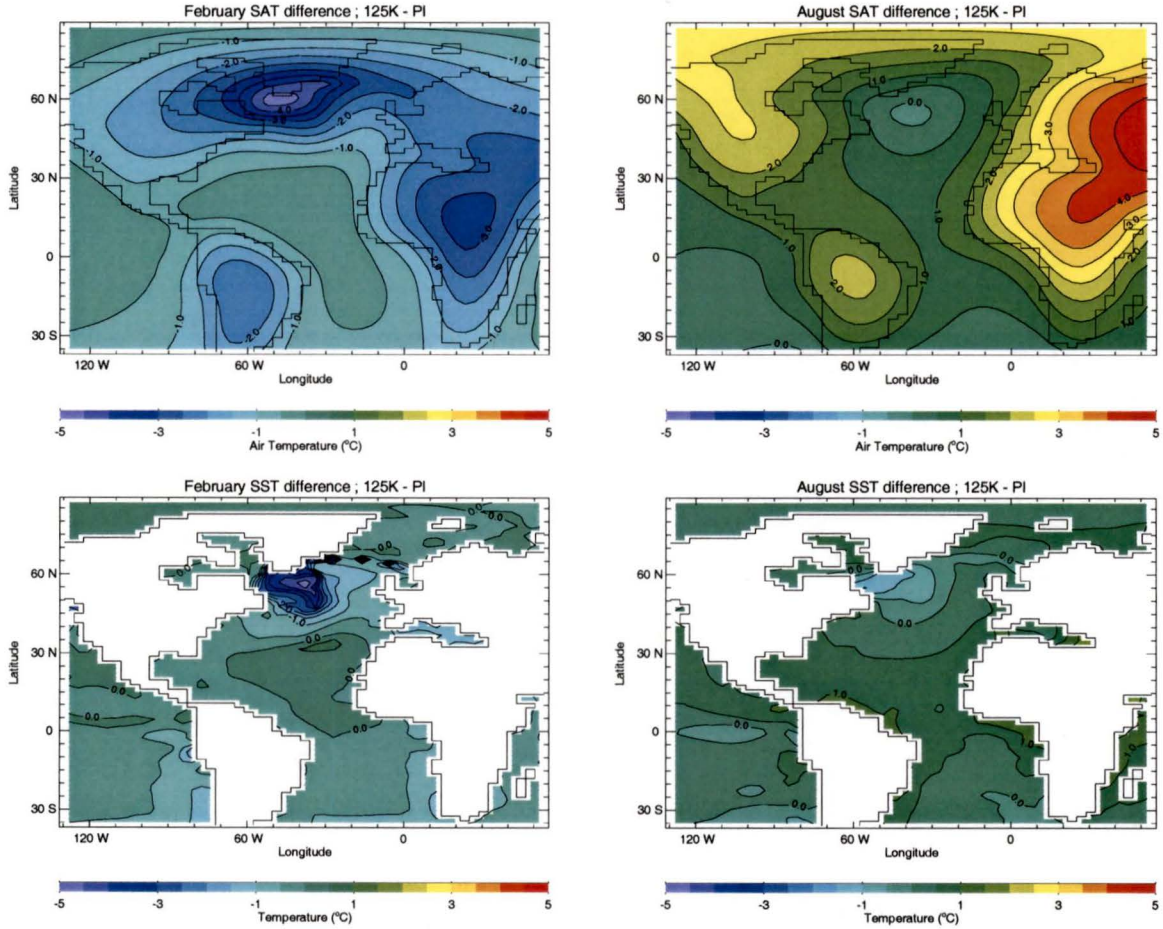

Figure 3.7: **February (left) and August (right) monthly mean SAT and SST differences for (*125K – PI*).**

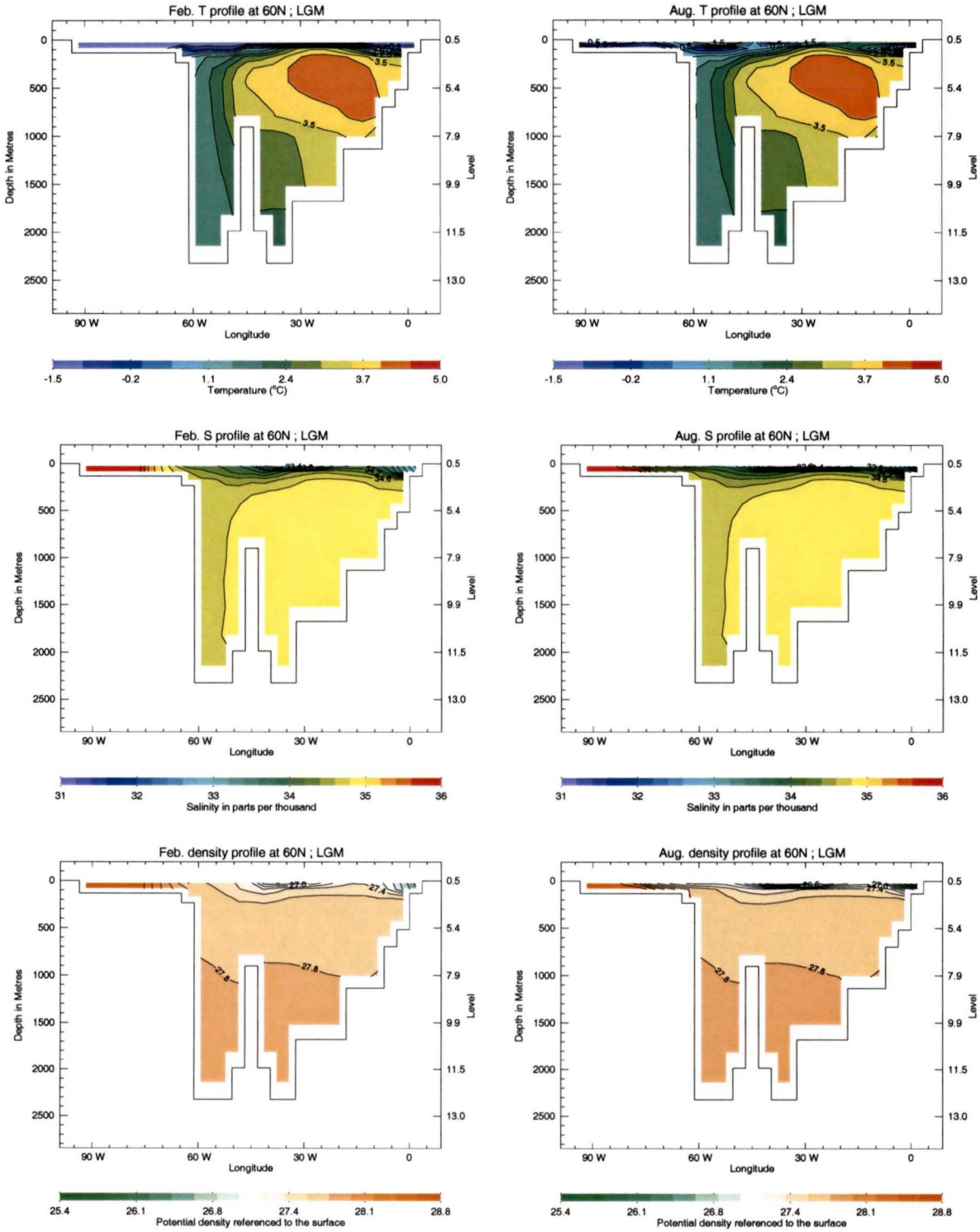

Figure 3.8: **LGM Temperature, Salinity and Density profiles at 71°N. Left column: February, right column: August.**

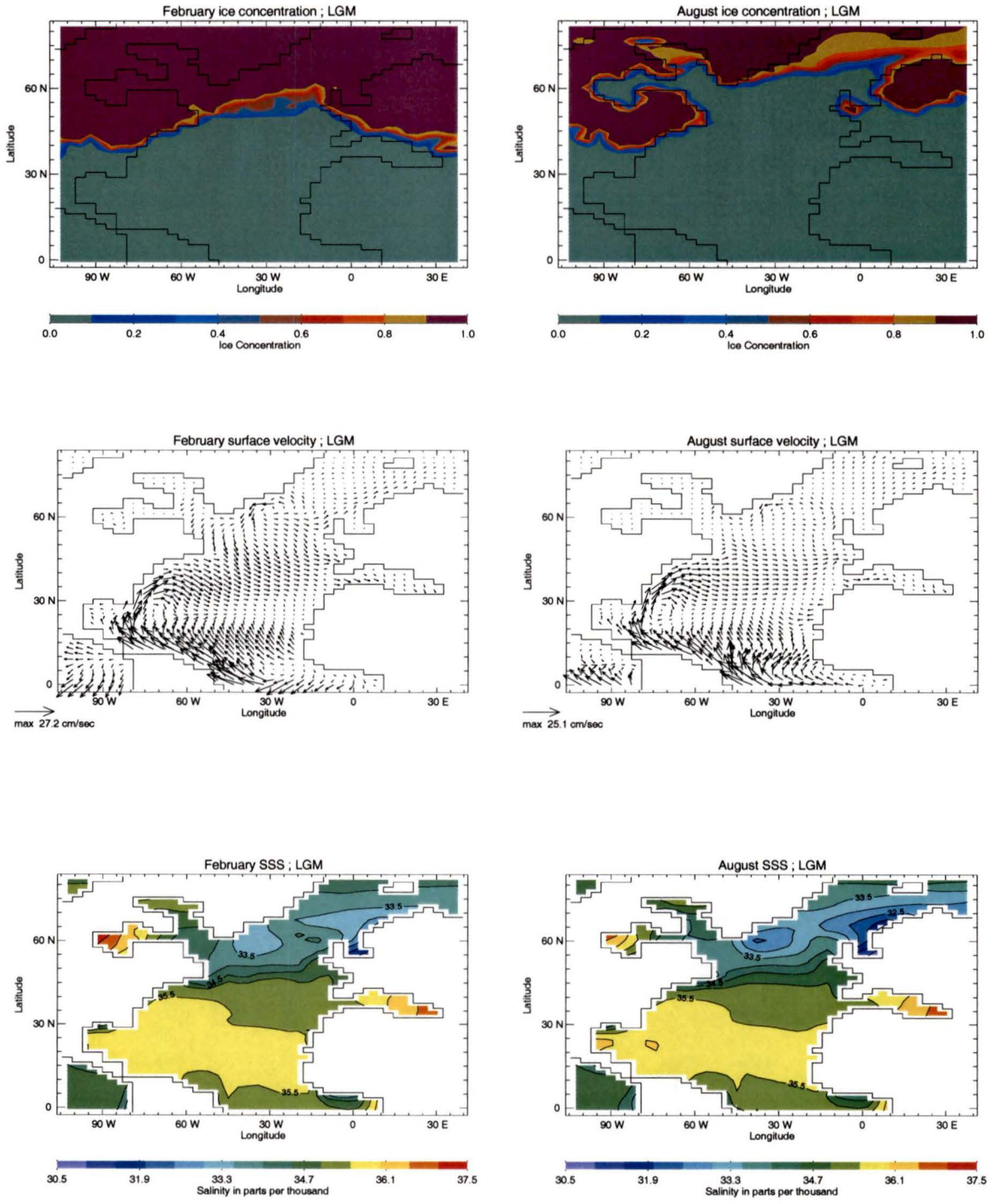

Figure 3.9: *lgm* **Febraury (left) and August (right) ice concentration, surface velocity and SSS.**

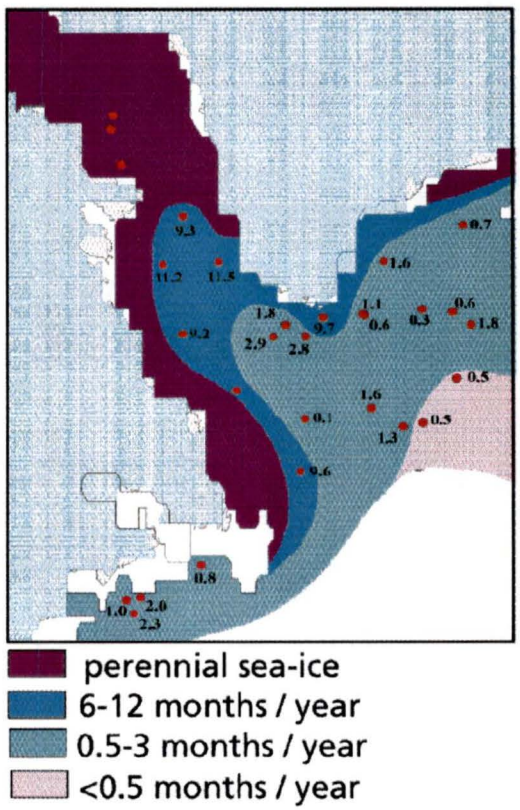

Figure 3.10: **North Atlantic sea ice paleo-reconstruction in LGM from de Vernal and Hillaire-Marcel (2000).**

Chapter 4

Inception of Modern Circulation

4.1 Introduction

From LS deep sediment core analysis, Hillaire-Marcel et al. (2001) suggested that during the last interglacial, NADW was fed only by DSOW without convective processes occuring in the LS. After the last interglacial period, the climate fell into a glacial period from 115 kbp to 14 kpb with a maximum ice extent at 21 kbp (LGM). During the LGM, de Vernal et al. (2002) suggested a weak thermohaline circulation without any convective processes north of 50°N. During the glaciation, the system underwent a succession of short warm interstadial states and longer cold stadial states. In the first chapter it was shown that the paleoclimate community agrees with the idea that these changes go along with variations of the oceanic circulation, particulary deep water formation in the northern North Atlantic. The cold stadial mode is associated with a shallow and weak North Atlantic meridional cell, while a stronger and deeper meridional overturning cell is expected during the warmer states. Not much is said about location of the deep water formation. Hillaire-Marcel et al. (2001) suggest that the formation of deep water by winter convection in the LS, like the modern situation, never occurred until the Holocene at about 8 kbp, a few thousand years after the deglaciation.

The simulations conducted in the last chapter support the hyppothesis that the LS convection did not happen in the Eemian, or in the LGM. In this chapter the inception of LS convection is tested by running equilibrium integrations at different times between 12 kbp and 6 kbp.

4.2 Results

The previous chapter showed that the thermohaline circulation is sensitive to variations in orbital parametres which change the sea ice cover during the winter at high latitudes, and to variations in CO_2 concentration influencing the global temperature and modifying the freshwater transport. The LGM occured at 21 kbp when the orbital parameters provided a minimum insolation in the NH summer, then it increased leading the climate to the present

interglacial (fig. 2.1**a**). Maximum summer insolation occured at 12kbp before decreasing again to the present value. In this section, experiments are run at different times after the deglaciation, between 12 kbp and 6 kbp, using paleo concentrations of CO_2 described in chapter 2. The minimum value used is 243 *ppm* at 12 kbp and the maximum value is 270 *ppm* at 6 kbp.

As this version of the model does not include a dynamic ice sheet component, the changes in the oceanic circulation, in the equilibrium integrations, come from variations of the orbital parameters and CO_2 concentration. However, all the Holocene integrations produce the same oceanic circulation characteristics and global mean temperatures as the pre-industrial: the mean SAT varies between 17 and 17.4 °C; the maximum meridional overturning stream function oscillates between 21 and 21.4 Sv; the water always sinks to the bottom of the basin creating a deep meridional cell. Moreover, winter convection occurs in the Irminger Sea and in the LS for each experiment.

The changes in the orbital parameters compared to present, are not important enough to modify the sea ice cover in the LS which would inhibit the convective processes. The CO_2 concentration is not low enough to reduce the freshwater export and generate a low density ocean surface that would stop the convective processes. Yoshimori (2001) conducted a sensitivity study with the UVic Earth System Climate model, and found a CO_2 concentration threshold between the glacial and modern oceanic circulation modes. This threshold stands between 200 *ppm* and 280 *ppm*. Here the integrations were run with CO_2 concentration ranging from 243 *ppm* to 270 *ppm* and they all produce a modern oceanic circulation. The results allow us to restrain the limits of the threshold from 200-280 *ppm* to 200-243 *ppm*.

These results do not apparently support the hypothesis of Hillaire-Marcel et al. (2001) concerning the onset of a modern like situation around 8 kbp. It is important to realise that the inception of a modern-like oceanic circulation in the Holocene is being simulated with equilibrium runs although it is in reality a transient state between glacial and modern modes. During the deglaciation, as described in the first chapter, the climate was highly unstable, oscillating between stadial and interstadial modes on time scales of a thousand years or so. These rapid changes were mainly due to the input of fresh water coming from the Laurentide and Fennoscandian ice sheets, followed by atmospheric and oceanic feedbacks. As dynamical ice sheets are not included in this version of the model, it is natural that the simulations tend to approach either the modern equilibrium mode or the glacial mode.

The perpetual forcing runs are efficient in reproducing the climate system in a relatively stable state, like the present and the last interglacial or the maximum glaciation. Nevertheless, it is not adequate to simulate transient states. The results obtained here show that

the climate does not respond only to orbital prameters and CO_2 concentration forcing, but also to rather more complicated feedbacks from continental ice sheet melting, such as ice albedo, elevation and fresh water runoff, which are not included in the model. In this case, to simulate a deglaciation climate, the fresh water coming from ice sheets melting is obviously a fundamental component of the system. The next section briefly describes another integration run from the LGM to the present day including fresh water forcing from the Laurentide ice sheet melting.

4.3 Aside

Aside from the perpetual forcing runs, a long integration from the LGM to the present was run. The insolation varied and the CO_2 concentration followed the forcings described in chapter 2. The changes in ice sheet height and extent was taken from reconstructions of Peltier (1996). The ice sheet is represented in the model by a local increase in elevation and in albedo. In addition, Licciardi et al. (1999) provide data for the freshwater origining from the melting of the Laurentide ice sheet. This freshwater entered the North Atlantic by the Mississippi River, the Saint Lawrence Estuary, the Hudson River, the Hudson Strait and the Canadian Arctic. The mean ocean salinity was increased by 0.6 *psu* at the begenning of the integration to reach the modern value after the fresh water forcing was added.

Time series of the CO_2 forcing, the freshwater forcing and the maximun North Atlantic overturning streamfunction are displayed in Figure 4.1. The overturning starts at 10 Sv at the LGM, collapses during the deglaciation between 17 kbp and 15 kbp during the first input of fresh water in the ocean. The fresh water forcing continues to increase, reaches a maximum at 10 kbp and decreases until 7 kbp. During this period, the North Atlantic overturning remains shut down. After the fresh water forcing stops, the overturning rapidly resumes between 6 and 5 kbp, when the ice sheet has totally vanished. This result is in agreement with Hillaire-Marcel et al. (2001) and shows that once the appropriated component is included in the system, the model is able to reproduce the oceanic circulation deducted by the proxy reconstructions. However, in this simulation only the freshwater coming from the melting of the Laurentide ice sheet has been included. With freshwater also coming from the Fennoscandian ice sheet melting to the Nordic Seas, the result would probably be different and the oceanic circulation might not be able to recover. Nevertheless, this simulation shows that the oeanic circulation in the model is very sensitive to fresh water input to the North Atlantic.

From the last two chapters, the model has shown the ability to react to different forc-

ing considerably different from present. The oceanic circulation and particularly the deep water formation in the northern North Atlantic is sensitive to variations in the radiative forcing induced either by orbital parameters or CO_2 concentration changes. These changes ultimately lead to variations in fresh water fluxes at the surface of the ocean that modify the circulation. As the model has been able to reproduce different modes of deep water formation relating to paleo- external forcings, it is reasonable to attempt to simulations of future climate with higher CO_2 concentrations.

Wood et al. (1999) predict a cessation of deep water formation in the LS while the circulation remains activated by the overflow water under a global warming climate. The variation of deep water formation in the North Atlantic in a global warming climate with the UVic Earth System Climate Model is studied in the next chapter.

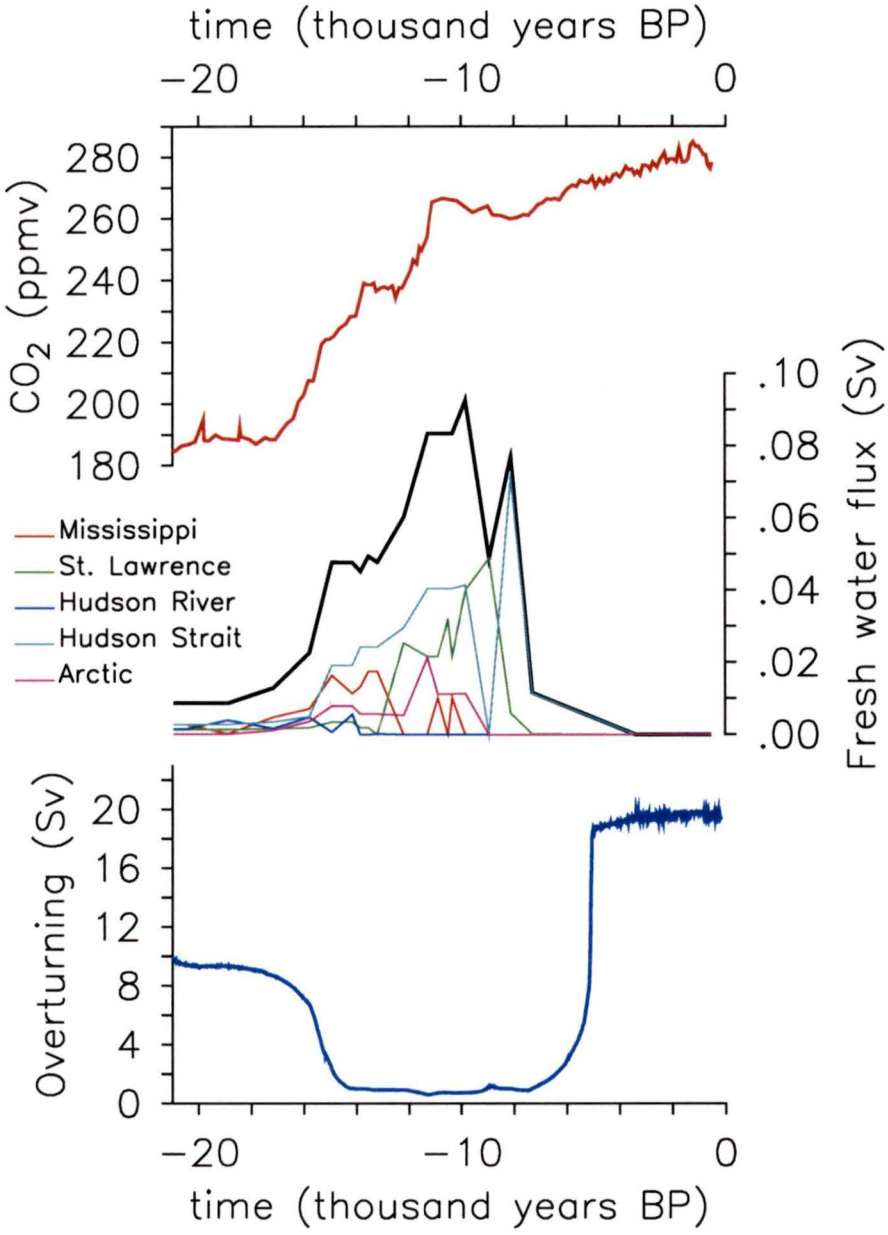

Figure 4.1: **CO_2 forcing, freshwater forcing and maximum North Atlantic overturning for the transient run from LGM to present.**

Chapter 5

Global Warming

5.1 Introduction

In the previous chapters, the evolution of the thermohaline circulation was surveyed over the last glacial cycle. In particular the variation of NADW formation through its two contributors, the LSW formed by winter convection, and the overflow water originating from the Nordic Seas. This last one is poorly represented in the model, which is a recurrent problem in ocean GCMs of coarse resolution, because of the small scale processes involved. Consequently the deep water formation occurs by convection above the Iceland-Scotland ridge, in the Irminger basin. This shortcoming produces surface water in the Nordic Seas which is too cold and fresh with formation of seasonal sea ice inhibiting convective processes. Despite this discrepancy, the model succeeds in representing different modes of oceanic circulation under different boundary conditions. This includes variations in the meridional overturning strength and variations in the location of deep water formation, as expected from proxy reconstructions. As the changes in deep water formation in the model have been successful for radically different past climate states, it gives some confidence in the ability of the model to produce different climate states, thus making it viable for use in future climate projections. It is therefore reasonable to investigate a potential re-organisation of the ocean circulation under high CO_2 concentrations expected in the future.

Over the next century, carbon cycle models project atmospheric CO_2 concentrations to increase to values between 540 to 960 *ppm* (or 490 to 1260 *ppm* including uncertainties) (IPCC 2001). Many modelling studies have been performed to predict future climate conditions with increasing greenhouse gases. All of them agree upon a global warming, although a wide range of uncertainties persists. One half of these uncertainties arises from the emission scenario and the other half from climate feedbacks. The global temperature is predicted to increase by 1.4 to 5.8°C (IPCC 2001) over the next century.

The ocean, with its large heat capacity and inertia acts as a climate regulator. The ocean circulation therefore has an important role in the global warming process. In modelling studies, the thermohaline circulation appears to be very sensitive to the atmospheric CO_2 concentration. Some studies predict it to collapse (Manabe and Stouffer 1993, 1999) due

to low surface density under warm conditions allowing more fresh water transport by the atmosphere to high latitudes. This would lead to strong stratification of warm and fresh water in the North Atlantic. Further studies indicate a dependence upon the CO_2 increase rate (Stocker and Schmittner 1997). A rapid increase would make the system collapse, whereas a moderate one would allow the system to to recover to a lower level after an initial drop.

In this chapter the evolution of the formation of deep water in the North Atlantic under high CO_2 concentrations with the UVic climate model is examined. First, three equilibrium experiments with perpetual forcing of high CO_2 concentrations, comparable to the experiments conducted in the previous chapter, have been integrated. Second, three integrations with CO_2 varying have been conducted in order to compare them with other studies and to try to understand the transient states linking one equilibrium to another.

5.2 Results

5.2.1 Equilibrium runs

Yoshimori (2001) using the UVic Earth System Climate Model, showed that the thermohaline circulation in the model is sensitive to both variations in orbital parameters and CO_2 concentrations. He demonstrated the presence of a CO_2 concentration threshold standing between 200 and 280 *ppm*. In the last chapter, this threshold has been restrained between 200 and 243 *ppm*. With CO_2 under the threshold, the ocean circulation is in a glacial mode, with a shallow and weak meridional North Atlantic overturning cell. With CO_2 above the threshold, it is in the modern mode. He showed that under these low CO_2 concentrations, the variations of SST induce variations in seasonal sea ice cover acting on the SSS, which partly governs density gradients responsible for the variations of deep water formation.

In this section, the sensitivity of the thermohaline circulation to high CO_2 forcings is investigated. Five equilibrium integrations have been conducted with present day orbital forcing and constant atmospheric CO_2 concentrations becoming larger from one simulation to the next. The simulations and their respective CO_2 concentrations are:

- PI : $CO_2 = 280$ *ppm*
- PD : $CO_2 = 350$ *ppm*
- $GW6$: $CO_2 = 600$ *ppm*
- $GW9$: $CO_2 = 900$ *ppm*

- *GW12*: $CO_2 = 1200\ ppm$

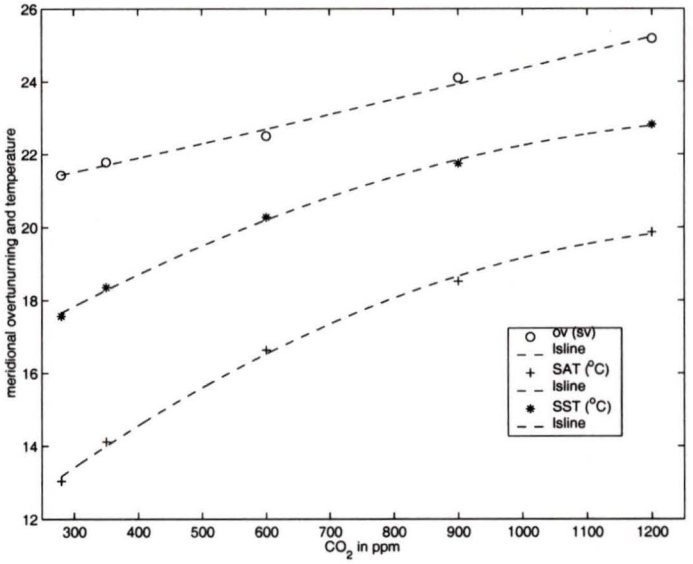

Figure 5.1: **Annual means for: maximum overturning stream function in the North Atlantic, SAT and SST under different CO_2 forcings. The dashed lines represent a the 2^{nd} order polynomial fit to the data.**

Figure 5.1 shows the response of the maximum North Atlantic meridional overturning, SST and SAT to CO_2 increase. Contradicting studies using transient CO_2 increase which find a weakening or collapse of the thermohaline circulation (Stocker and Schmittner 1997, Wood et al. 1999, Rahmstorf 1999), here the equilibrium meridional overturning increases linearly with the CO_2 concentration. However SST and SAT do not respond linearly, as shown by the dashed lines representing the second order polynomial fit between the different runs. When CO_2 increases by 70 *ppm*, from 280 to 350 *ppm*, SAT rises by 8.3%; while for a 300 *ppm* increase (from 900 to 1200 *ppm*), SAT increases only by 6.8%. However, the climate sensitivity of 3°C for doubling CO_2 agrees with other studies (IPCC 2001).

Figure 5.2 shows the maximal convection depth in February (left), and the mean annual North Atlantic meridional overturning stream function (right). From top to bottom equilibrium CO_2 atmosphere levels increase from 280 *ppm* to 1200 *ppm*. The convection maps show that deep water formation remains active both in the LS and in the Irminger Sea in all the simulations. In *PI* and *PD*, LS convection occurs south of the south-western tip of Greenland and reaches the bottom at 2000 *m*. As CO_2 increases, the site shifts north-westward in the basin and becomes slightly shallower. In the Irminger Sea,the convection site expands north-eastward and also becomes shallower with increasing CO_2 concentrations.

The consequences of these variations are visible in the North Atlantic meridional overturning graphs. In *PI* and *PD*, the core of the overturning cell occurs at 58°N and the NADW sinks to the bottom of the basin to 4500 m producing a global meridional overturning cell with a mean depth of 3000 m. In the *GW* simulations, as CO_2 increases, the core of the meridional overturning cell shifts northward to 61°N, and the NADW ceases to sink to the bottom. The NADW cell is 1000 m shallower, with an avarage depth of $\sim$ 2000 m.

In the winter with low CO_2 concentrations, the high latitudes cool down very efficiently. The incoming solar radiation is nul or low, the outgoing longwave radiation is then the principal mechanism for radiative transfer, which produces a high energy loss. When CO_2 concentrations become higher, the outgoing longwave radiation is reduced, which in turn substantially reduces the energy loss and the winter cooling at high latitudes. The February SAT, SST and maximal sea ice extent differences between *GW12* and *PI* are displayed in figure 5.3. It is seen that the high latitudes warm up more than the tropics, by 3°C in the atmosphere and 1.5°C at the ocean surface in the North Atlantic. The reduced winter cooling induces a retreat of the maximum sea ice extent making the LS and the Nordic Seas ice free in February. It can be noticed that the northward shift of the convection sites observed in figure 5.2 follow the displacemenent of the ice edge (fig. 5.3). This indicates that the variation of the location site of deep water formation is a consequence of the variations in sea ice extent.

Figure 5.4 represents latitudinal profiles of temperature, salinity and density across the North Atlantic at 64°N. The profile is marked by red line in figure 5.3. From West to East, it crosses the LS (1000 m deep), Greenland, the Irminger Sea (1500 m deep), the Iceland-Scotland ridge (1000 m deep) and the south part of the Nordic Seas. *PI*, in the left column, has a fresh and cold buoyant lid developing from the west side of the LS and in the Nordic Seas due to the presence of seasonal sea ice. In *GW12* (right column) the vertical stratification breaks down due to the absence of sea ice, allowing intense convection. The water properties are very different between the two runs. The temperatures along the transect are about 5°C warmer in *GW12*. The salinity in *GW12* is 0.1 *psu* higher in the LS and the Nordic Seas, while it is about 0.3 *psu* higher in the Irminger Sea and above the ridge. The large variations in temperatures between *PI* and *GW12* lead to a large density differences visible in the bottom panels. In *GW12*, the water convecting is 0.3 units lighter in the LS and up to 0.6 units lighter above the ridge because of the warm water coming from the North Atlantic Drift. The low density of the warm water convecting in the Irminger Sea produces shallow convection, responsible of the shallow overturning cell.

The northward shift of the deep water formation sites and the shallowing of the merid-

ional overturning cell are the consequence of reduced winter cooling at the pole, shrinking the maximum sea ice extension and generating relatively warm deep water convecting farther north.

The physical processes responsible for the intensification of the meridional overturning with high CO_2 concentration were explained in Weaver et al. (2001). They used use the zonally-averaged depth-integrated steric height. The steric height is a measure of depth-integrated pressure above a reference level. It qualitatively represents a cumulative density anomaly in the vertical direction. The lower the density is above the reference level, the higher the steric height. This makes the zonally-averaged depth-intergrated steric height at low latitudes higher than the zonally-averaged depth-integrated steric height at high latitudes. Weaver et al. (2001) found a linear relation between the meridional gradient of zonally-averaged depth-integrated steric height from the south tip of Africa to the northern latitude of deep water formation and the North Atlantic meridional overturning. The steeper the gradient is, the higher overturning strength.
Variation in density due to variations in temperature and salinity is not a linear process. The density of warm water is more sensitive to variations in temperature while the density of cold water is more sensitive to variations in salinity. In the global warming case, the increased temperature at low latitudes has a strong influence on the density. The tropical water becomes very light compared to the polar water which steepens the slope of the meridional gradient in the depth-integrated steric height, and corresponds to an increase in the meridional overturning strength. In the present simulations the atmospheric moisture transport is accomplished only through diffusion. In global warming integrations with a parametrisation of moisture transport including advection, the precipitation increases at high latitudes, freshening the surface water (Weaver et al. 2001), and the overturning remains mainly unchanged.

When the CO_2 concentration is lower than 350 *ppm*, the high latitudes are cold enough (fig. 5.3) to maintain cooling of the North Atlantic Drift, which transforms the warm surface water into cold deep water. When CO_2 reaches 600 *ppm* the convective processes occur at warmer temperatures, producing lighter water and leading to a shallow meridional overturning cell and a steepened meridional steric height gradient. The overturning strength increases, leaving even less time for the surface water to cool down at high latitudes, acting as a positive feedback to warm up the high latitudes and making this state stable.

The nonlinear response of global warming to increasing CO_2 (fig. 5.1) can be explained by two different modes of thermohaline circulation separated by a CO_2 threshold standing between 350 and 600 *ppm*:

1- A modern mode with CO_2 lower than the threshold and intense cooling in high northern latitudes in the winter, leading to the formation of cold and deep NADW with a meridional overturning strength around 21 Sv. In this mode, the system warms up efficiently with CO_2 increase.
2- A global warming mode with CO_2 above the threshold and less winter cooling in high northern latitudes, (fig. 5.3). Consequently the seasonal sea ice extent is reduced and convection occurs farther north. Moreover, the water convecting at high latitudes is warmer and hence lighter, leading to a shallow and warm meridional overturning cell. Because of the high tropical temperatures, the meridional depth-integrated steric height gradient is steepened, leading to an intensification of the meridional overturning strength. In this mode the global temperature undergoes a more moderate temperature increase with CO_2 increase.

These findings can be related with the results of Yoshimori (2001) showing that in equilibrium runs when CO_2 increases, the overturning increases. He already found a CO_2 concentration threshold triggering the thermohaline circulation from a glacial mode to an interglacial mode when CO_2 increases from 200 *ppm* to 280 *ppm*, this range has been restrained to 200 *ppm* to 243 *ppm* in the previous chapter. Here another threshold is found between 350 *ppm* and 600 *ppm* with the thermohaline circulation changing from a modern mode to a global warming mode.

In this section, the perpetual forcing runs provided information for sensitivity of the thermohaline circulation to different CO_2 concentrations in equilibrium state. However in global warming projections, the interest is on the reaction of the climate system to a continously varying forcing that has never been observed in the past, *i.e.* the rapid CO_2 increase. To investigate the reaction of the NADW formation in the model to a gradual CO_2 increase, three transient integrations have been run and are examined in the next section.

5.2.2 Transient runs

Introduction

Wood et al. (1999) using the Hadley Centre coupled atmosphere ocean GCM with sufficient resolution to obtain deep water formation from Denmark Strait Overflow Water, performed two simulations with CO_2 starting from pre-industrial values and increasing at rates of 1% and 2% per year. In these expriments, the thermohaline circulation ceased in the Labrador Sea, while deep water formation persisted in the Nordic Seas, independent of the CO_2 increase rate. As the climate warmed, the DSOW became warmer and

hence lighter. The density contrast between the DSOW and the deep LS water was then reduced. This made the deep circulation of the LS collapse, while DSOW remains unchanged. This uncoupled bipolar source of NADW displayed the same behaviour as presented from paleo-reconstructions by Hillaire-Marcel et al. (2001) for the last interglacial period and successfully simulated by the UVic climate model in chapter 3.

In this section, three simulations with transient CO_2 increase are performed. *1PC* and *2PC* begin in 1999 from the *PD* simulation which is the modern equilibrium run with an atmospheric CO_2 concentration of 350 *ppm*. In *1PC*, CO_2 is increased by 1% per year until 2100 when it reaches 960 *ppm* and is held constant until 2700. In *2PC*, CO_2 is increased by 2% per year until 2070 when it reaches 1390 *ppm* and is also held constant until 2700. The third transient run, *GHG*, begins in 1850 from *PI*. The initial CO_2 concentration of 280 *ppm* is increased according to the formulation in Weaver et al. (2000), so that CO_2 follows the historical concentrations of anthropogenic greenhouse gases from 1850 to 1998. The same formulation is maintained from 1998 to 2100 and remains close to the 1% increase rate. From 2100 to 2700 CO_2 is held constant at 1008 *ppm*. The variations of CO_2 concentrations for each experiment are plotted on the top panel of figure 5.5.

Results

The second panel of figure 5.5 represents the time series of the maximum mean annual North Atlantic meridional overturning for the three integrations, while the third panel is the time series of the global annual SAT and SST. In all the runs, the overturning drops and temperatures rise when CO_2 increases, in agreement with previous studies (IPCC 2001). Once the CO_2 forcing is relaxed, the overturning recovers in about two hundred years, and surpasses its initial value, while the temperatures stabilise. The overturning strength and temperatures reached at the quasi-equilibrum, in 2700, fit with those found in the *GW* runs (fig. 5.1).

The February convection depth and mean annual North Atlantic meridional overturning of the transient runs once CO_2 has reached its maximum values, are displayed in figure 5.6. Convection ceases in the LS in all of the integrations. The third row in the figure is for *2PC* after 60 years of integration, when the CO_2 concentration is similar to that in *1PC* in 2100. It should be noted that independent of the CO_2 increase rate, both experiments reach the same state (overturning = 19 Sv and have the same convection site) when CO_2 reaches 960 *ppm*, which is in agreement with Wood et al. (1999). In *GHG*, when CO_2 reaches 1008 *ppm*, the overturning strength of 18.3 Sv is slightly lower than in *1PC* and *2PC* with CO_2 concentrations of 960 *ppm*. Finally, in *2PC* when CO_2 reaches 1390 *ppm*, the overturning

drops to 17.7 Sv, but never ceases as it does in other simulations (Rahmstorf 1999). Despite the differences in the meridional overturning strength, the North Atlantic meridional cells look identical in each experiment. The core of the cell occurs at about 50°N, as it does in *PI* and *PD*. The mean depth of the meridional cell is about 2500 m, which is deeper than the *GW* equilibria, but shallower than the modern situation. Moreover in all the snapshots, the convection ceases in the LS but remains active in the Irminger Sea independent of the CO_2 increase rate, in agreement with Wood et al. (1999).

The February convection depth and North Atlantic meridional overturning stream function in the transient runs in 2700 are shown in figure 5.7, after the CO_2 forcing has been relaxed for 600 years. The convection maps show that weak convection is still active in the Irminger Sea and recover in the LS in all integrations. This contradicts the results of Wood et al. (1999), for whom the overturning is only driven by the DSOW under global warming conditions. Another point to note is that the meridional overturning function, for each run, shows the characteristics of the global warming mode described earlier for the *GW* equilibria. In this mode, the North Atlantic cell's core shifts northward to 60°N and becomes shallower, with a mean depth of $\sim$ 2000 m. Its strength increases with CO_2, reaching a maximum value of 25 Sv in *2PC*, which has the highest CO_2 concentration of 1390 *ppm*. Here again, it should be noted that in *2PC*, when CO_2 is held constant at 950 *ppm* (third row of fig. 5.7), it reachs the same equilibrium as in *1PC*,which has the same concentration, with a maximum North Atlantic overturning of 23.7 Sv. This observation shows again that the system is sensitive to the atmospheric CO_2 concentration, but not to its increase rate, in agreement with Wood et al. (1999).

An earlier study by Wiebe and Weaver (1999) using the UVic Earth Climate System Model found the same weakening of the North Atlantic overturning during the transient state and subsequent re-establishment to a higher level than initially. Wiebe and Weaver (1999) explained this behaviour by an increased hydrological cycle in the warmer climate which is a direct consequence of the Clausius-Clapeyron relation. This leads to more evaporation in the tropics and enhanced precipitation at high latitudes. The surface water at the convection sites then becomes more fresh, which reduces the surface density and subsequently the overturning strength. In this process, the ocean acts as a negative feedback to the warming of the high northern latitudes, through a low overturning exporting less heat to the high latitudes. When CO_2 ceases to increase, the climate system is allowed to approach an equilibrium. The overturning transports anomalously warm water to high latitudes, forcing the ice edge back. Once the ocean is ice free, the fluxes to the atmosphere are restored, allowing surface water to cool down and resume the overturning. This process

acts as a positive feedback, maintaining the circulation at warmer temperatures. These processes explain the weakening and subsequent re-establishing of the overturning strength. In the present case however, the focus is on the variations of the convective processes in the LS.

Why does the convection collapse and resume in the Labrador Sea ?

Figures 5.6 and 5.7 show that the convection in the LS stops and resumes in each experiment. To understand this phenomenon the *GHG* run is analysed. The figures displayed in this section contain the initial conditions (year 1850, $CO_2 = 280$ *ppm*), the end of the transient period (year 2100, $CO_2 = 1008$ *ppm*) and the end of the CO_2 forcing relaxation period (year 2700, $CO_2 = 1008$ *ppm*).

First, to examine the cause of the cessation of convection in LS, observed in all the transient runs, the initial conditions and the transient state of *GHG* are compared. The increased CO_2 concentration reduces the outgoing longwave radiation and efficiently decreases the winter cooling in high latitudes. Consequently, from 1850 to 2100, the maximum sea ice extension is forced back (fig. 5.8). Figure 5.9 represents latitudinal profiles of temperature, salinity and potential density across the North Atlantic at 64°N. The initial conditions in the left column, are compared with the transient state in the middle column.

On the East side of the profile, in the Nordic Seas, the sea ice retreat allows a further penetration of the North Atlantic Drift, breaking down the vertical stratification and allowing convection further East in the Nordic Seas. Figure 5.8 gives the February surface velocities. In 2100 compared to 1850, the North Atlantic Drift penetrates further towards the northeast on the southern border of the Nordic Seas due to the sea ice retreat. Then, the Irminger Gyre previously confined to the Irminger Sea, is widened on its east side which, combined with the enlargment of the convective site (fig. 5.6), tends to reduce the intensity of the Irminger Gyre along the Greenland coast. As a result, the Irminger Current, previously nourishing the LS with salty water, is weakened. The LS stays isolated from the North Atlantic Drift and its surface remains cool and fresh due to the sea ice melting. The latitudinal profile at 64°N (fig. 5.9) shows this relatively cold and fresh lid in the LS creating a strong vertical stratification and inhibiting the convective processes. The profiles show that in the LS and the Irminger Sea, from 1850 to 2100, the salinity increases by 0.1 *psu* and the temperature by 1.5°C. The water convecting is then 0.2 units lighter, explaining the shallow meridional overturning cell.

The left column of figure 5.10 represents the difference in evaporation, SST and SSS between 2100 and 1850. The precipitation differences follow the same pattern as those in

evaporation, and are therefore not displayed. Four patterns are noticeable on these maps. First, the largest differences occur across the west side of the Nordic Seas where the ice edge is forced back. From 1850 to 2100,the North Atlantic Drift penetrates further northeast, where the ocean surface becomes ice free, leading to higher temperatures, salinities and evaporation. The second pattern is a cell in the south of the Irminger Sea, with a negative evaporation and small temperature increase compared to the surroundings. This pattern comes from the reduction of the Irminger Gyre (fig. 5.8) bringing less North Atlantic Drift water but more fresh and cold diluted water coming from the ice edge melting in the Nordic Seas. The difference between the ocean surface and the air temperature is then attenuated, explaining the reduction of evaporation and the relative slight warming. On the other hand, the third pattern off the south Labrador coast consists of a cell with particulary large temperature and evaporation differences. As the LS is isolated from the North Atlantic Drift, the cold southward surface Labrador Current (fig. 5.8) is also reduced. The Gulf Stream flowing northward along the North American coast is then allowed to extend farther north, before separating from the coast. The replacement of the cold surface water from the Labrador Current by warm surface water from the North Atlantic Drift produces the large temperature difference observed on the SST map off the Labrador coast. The ocean-air temperature contrast is consequently increased, giving rise to the evaporation. Finally, the weak Irminger Current (fig. 5.8) keeps the LS isolated from the North Atlantic water. For this reason the LS warms only slightly compared to the remaining ocean, and its surface is fresher than in 1850, due to ice melting responsible of the buoyant lid observed on the latitudinal profile, which inhibits the convection.

The independent behaviour of the LS compared to the rest of the northern North Atlantic is hence explained. As CO_2 rises, the winter sea ice extent is reduced, allowing the North Atlantic Drift to penetrate further northeast along the southern border of the Nordic Seas and expanding the convection site in the north-western North Atlantic. The Irminger Gyre is then weakened. The Irminger surface current usually provides the LS with warm salty water which leads to vertical instability upon cooling. With a weak Irminger Gyre, the Irminger Current is reduced and the LS is isolated from North Atlantic Drift water. Its surface remains fresh due to the adjacent ice edge melting and forms a strong vertical stratification inhibiting the convective processes.

Once the CO_2 forcing is relaxed, the already high temperatures slowly stabilize (fig. 5.5). Meanwhile the overturning intensifies, becomes shallower and the cell's core moves northward. The convective processes resume in the LS. The system is allowed to approach an equilibrium, which is comparable with the global warming mode described in the previous

section.

The maximum ice retreat shown in figure 5.8 is accomplished in about 200 years in which the entire LS and half of Baffin Bay become ice free. The melting cessation allows the surface temperature and the evaporation to increase in the LS as seen in the right column of figure 5.10. The SSS consequently increases and become sufficient to break down the buoyant lid (fig. 5.9) restoring the convective processes in the LS. The overturning increases and brings anomalously warm water to high latitudes. The sea ice limit is forced back in the south Nordic Seas along the European coast (fig. 5.8). It reaches an equilibrium about 300 years after the CO_2 forcing is relaxed. The North Atlantic Drift carries warm water farther into the Nordic Seas. Consequently the evaporation, salinity and temperature continue to increase at these locations as seen in figure 5.10.

The latitudinal profile in figure 5.9 shows that the fresh and cold buoyant lid retreat into in the Hudson Strait. In the LS, the temperature is 1°C higher in 2700 than in 2100 and the salinity remains constant providing deep water with a density 0.2 units lighter. In the Irminger Sea, the water is also 0.2 units lighter due to an increase in temperature by 3°C and an increase in salinity by 0.2 psu. This lighter water convecting farther north is responsible for the shallow meridional overturning cell which is similar to the one in the global warming mode.

With the increased overturning, the ocean transports more warm water to high latitudes and acts now as a positive feedback to the warming of high latitudes. This is seen in the SST difference between 2100 and 2700 where the warming north of 40°N is 1.5°C higher than in lower latitudes, whereas in the transient case the low latitudes were warming more than the high latitudes (fig. 5.10).

Conclusions

In these simulations the variations of the thermohaline circulation in the model seem particulary sensitive to the variations of convection in the LS. When the convective process ceases in the LS, the overturning decreases and the thermohaline circulation is only driven by the convection in the Irminger Sea. Once the convection resumes in the LS, the overturning strength increases anew. This result agrees with Wood et al. (1999) although in their experiments, the convection and meridional overturning strength do not recover once the CO_2 forcing is held constant. This is due to the different parametrisation of the atmospheric moisture transport in the models. In this version of the UVic climate model, the moisture is parametrised by diffusion only, which gives lower precipitation at high latitudes than when advection is used.

Finally,the independence of the thermohaline circulation to the time profile of CO_2 increase also agrees with Wood et al. (1999).

5.3 Conclusions

The convective processes are driving the deep water formation, hence the global oceanic circulation which regulates the climate. In the previous chapters, it has been seen that the convective processes in the model are sensitive to external forcing. They vary with increasing CO_2 concentrations.

In transient states, as CO_2 increases, the warming at high latitudes melts the sea ice cover. The ice retreat induces a north-eastward shift of the Irminger convection site which is in direct contact with the incoming warm North Atlantic Drift. The LS being a more confined environment, becomes isolated from the rest of the ocean and its surface water remains fresh due to sea ice melting. The convection process stops and the overturning consequently decreases. During the transient state this process acts as a negative feeback to the warming of high latitude because of the weak meridional heat transport related to the weak overturning. Once CO_2 is held constant, the system tends to reach an equilibrium in which the sea ice stops melting and leaves the LS ice free. In a global warming climate, the high temperatures favorise an intense evaporation which brings the surface salinity back to value sufficient for breaking down the vertical stratification and restoring the convection in the LS, hence allowing the overturning to increase. The heat transport to high latitudes is then restored and acts as a positive feeback to the high latitudes warming.

The equilibrium state depends on the CO_2 concentration only and not on its former increase rate. For concentrations under 600 *ppm* the ocean is in the modern mode with a deep and cold circulation. The global mean temperature is very sensitive to CO_2 increase.

When CO_2 is higher than 600 *ppm* the ocean is in the global warming mode with a shallower and warmer deep circulation. The global mean temperature becomes less sensitive to CO_2 increase.

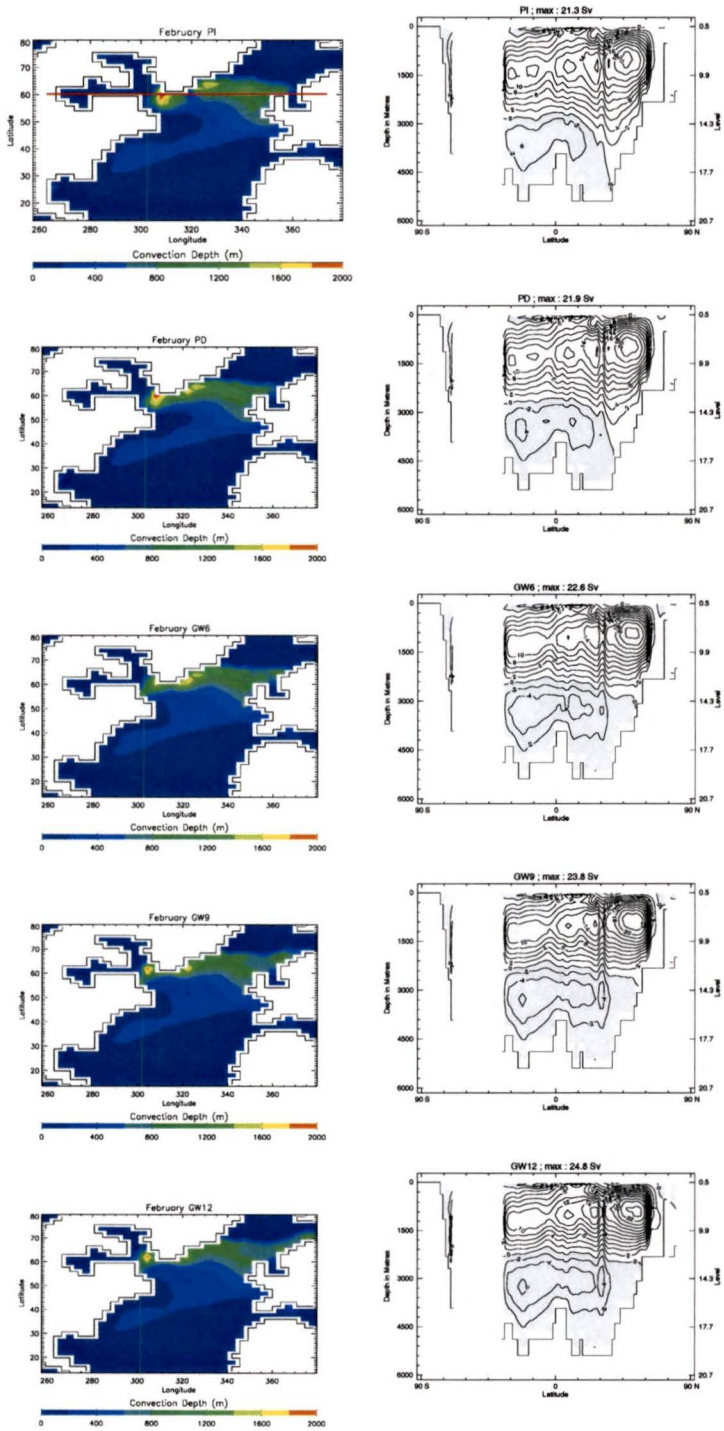

Figure 5.2: **February convetive depth in m (left) and annual North Atlantic meridional overturning in Sv (right). From top to bottom: PI, PD, *GW6*, *GW9* and *GW12*.**

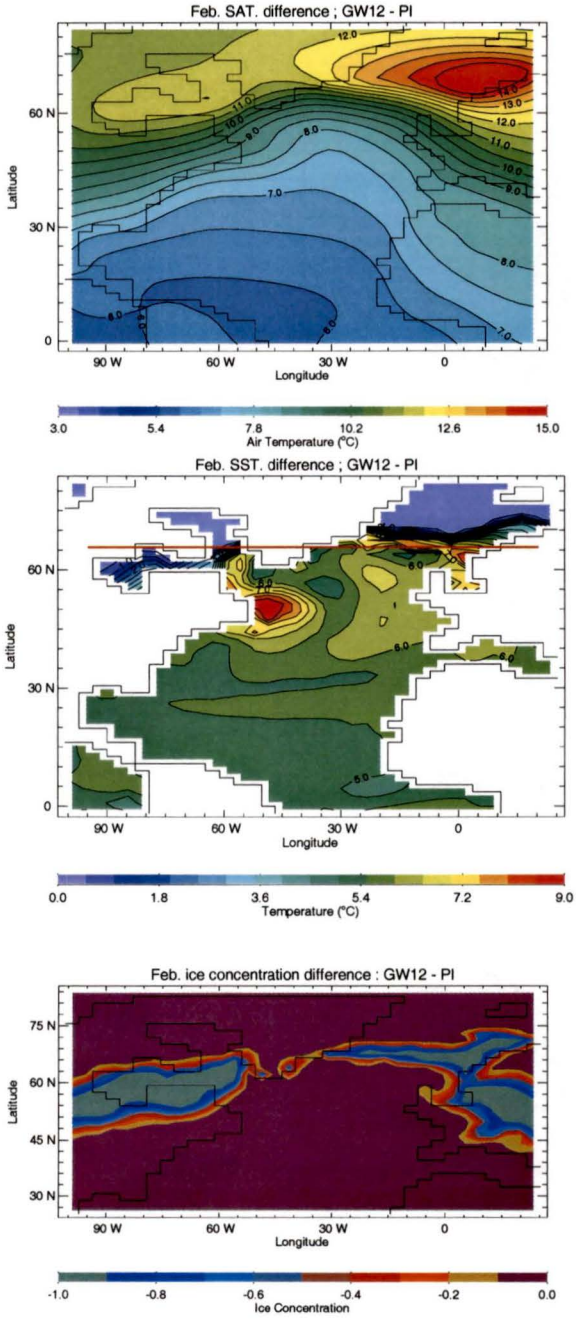

Figure 5.3: **February SAT, SST and sea ice concentration differences between *PI* and *GW12*. The red line in SST indicates the position of the 64°N latitunal profiles**

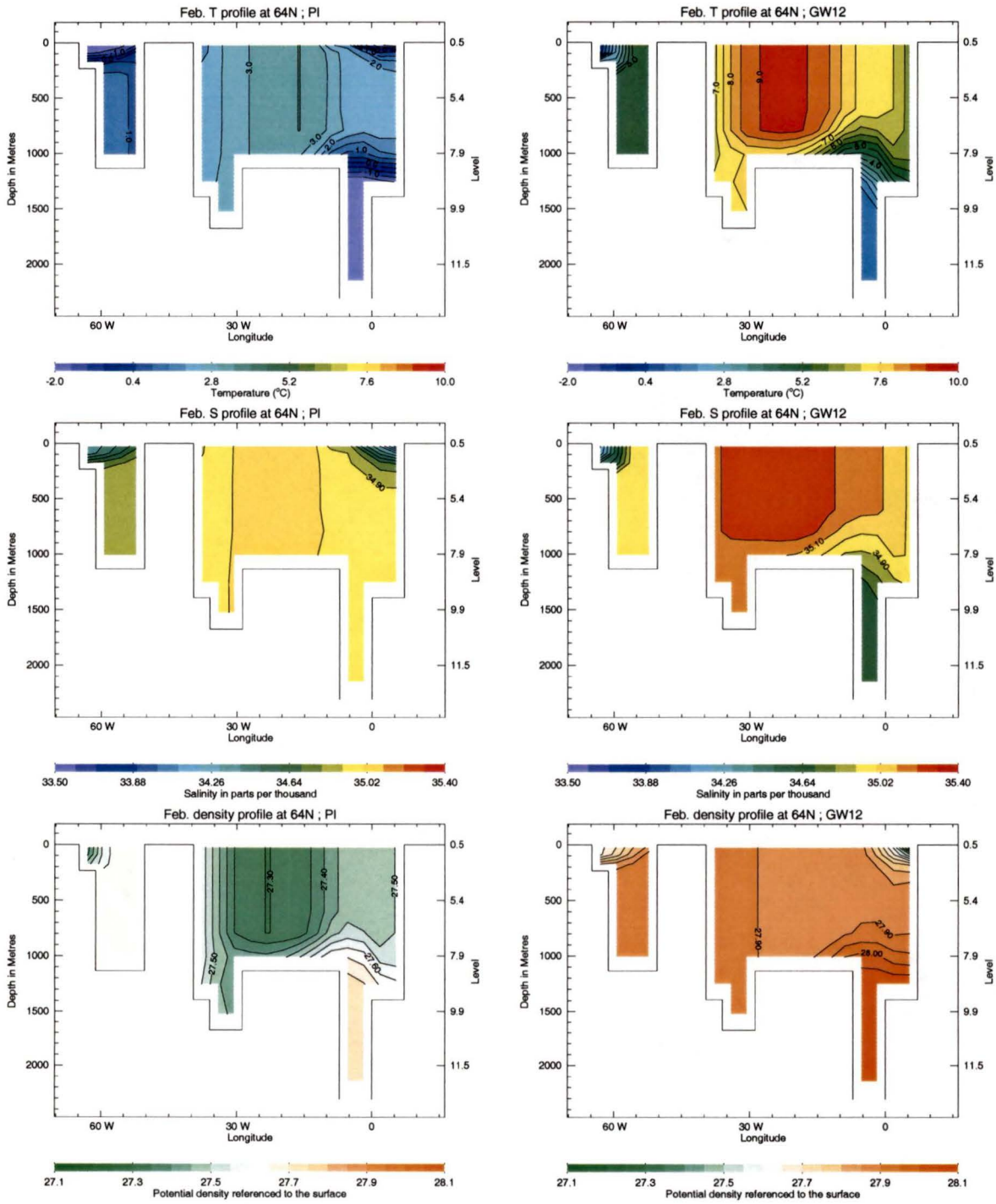

Figure 5.4: **Longitudinal profiles across 64°N of temperature, salinity and density for *PI* (left) and *GW12* (right)**

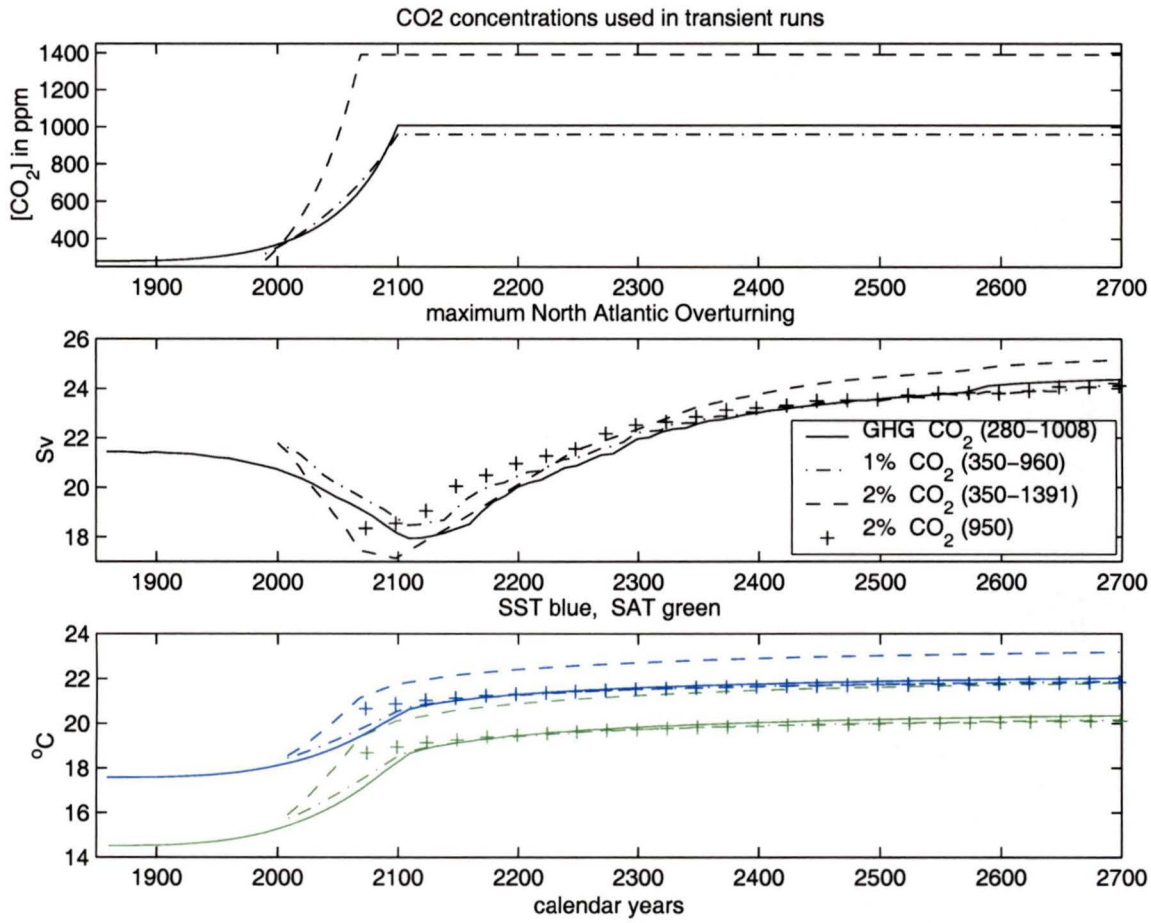

Figure 5.5: **CO_2 variation, Maximum North Atlantic overturning and SST, SAT in the transient runs. The crosses are values from run 2PC with CO_2 forcing relaxed at year 2060 when CO_2=950** *ppm*.

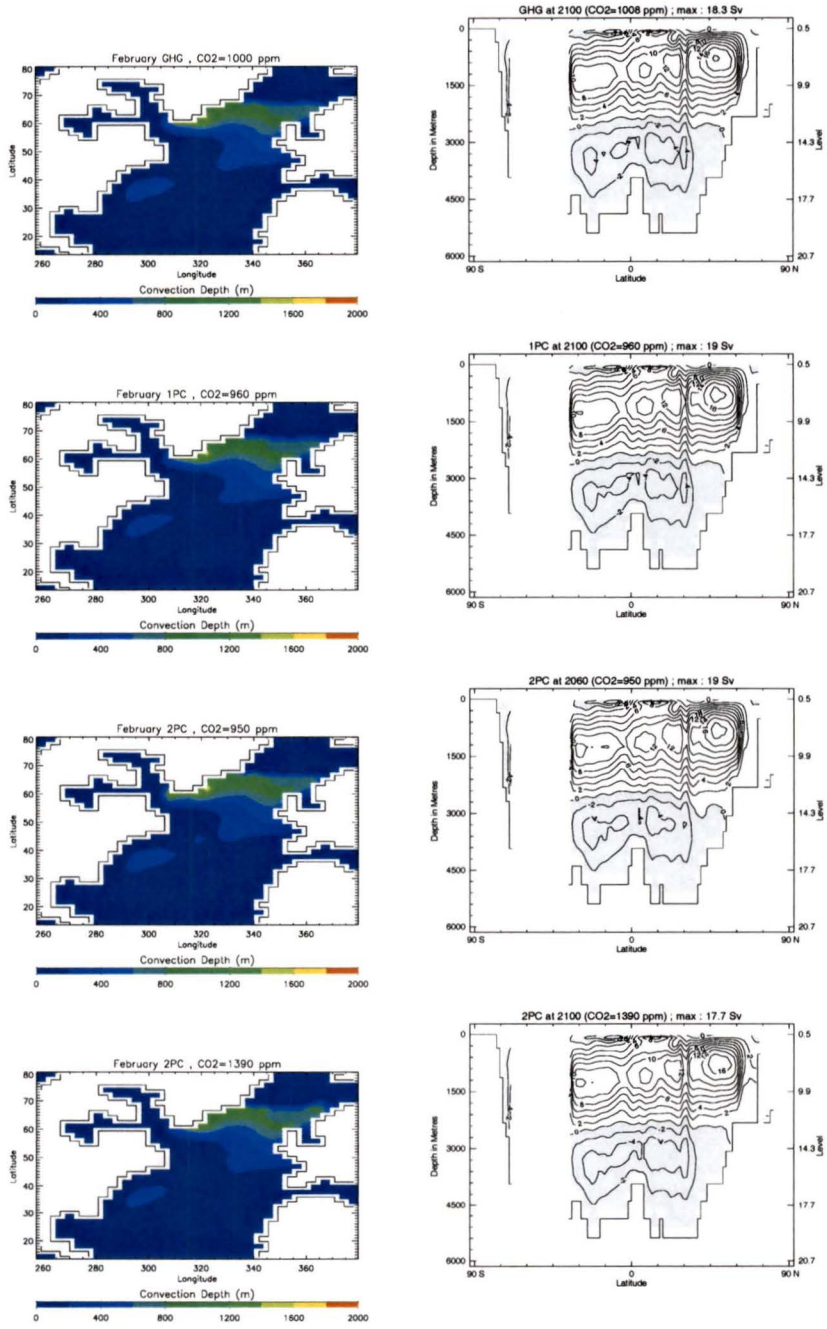

Figure 5.6: **February convetive depth in m (left) and annual North Atlantic meridional overturning in Sv (right) for the transient runs once CO_2 reaches its maximum. From top to bottom: *GHG*, *1PC*, *2PC* with CO_2=950 *ppm* and *2PC* with CO_2=1390 *ppm*.**

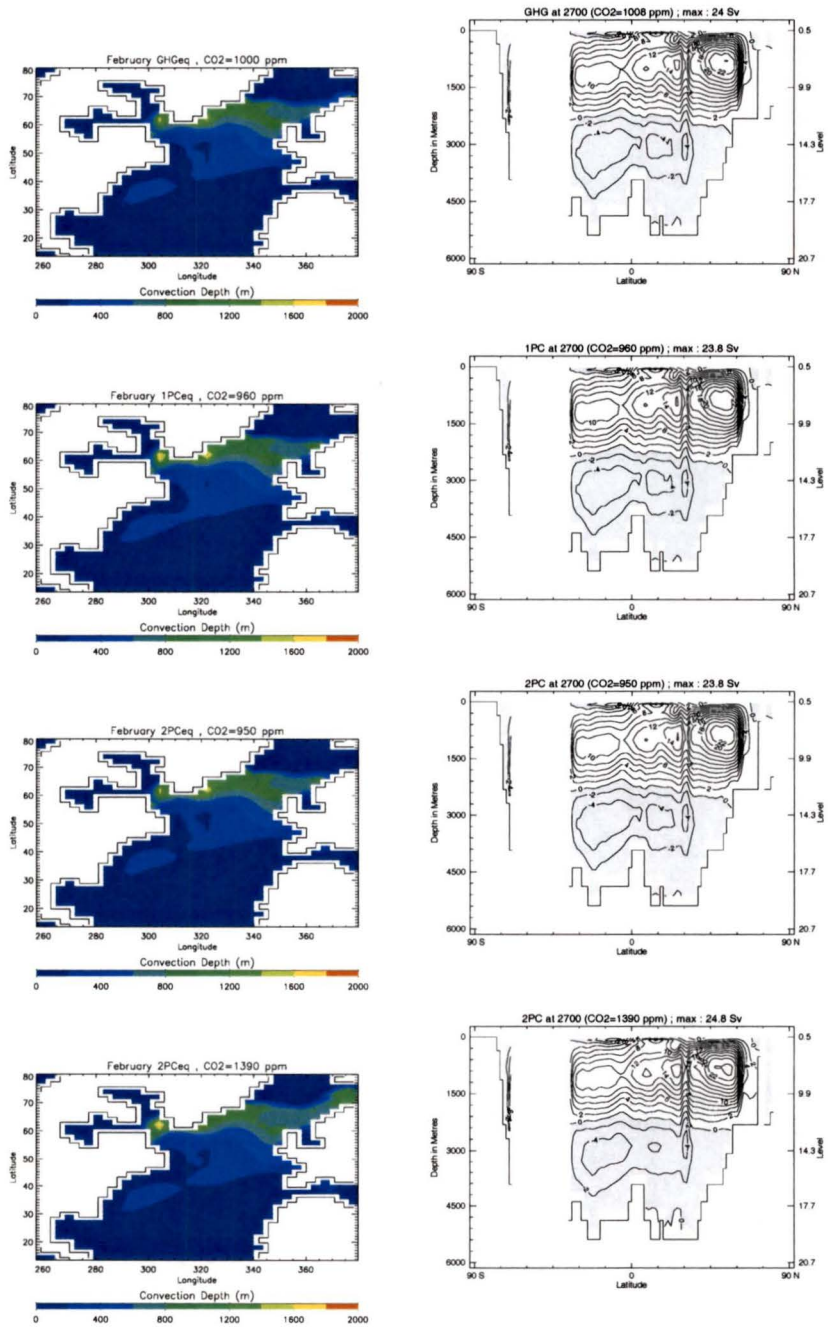

Figure 5.7: **idem as figure 5.6 for transients runs 600 years after the CO_2 forcing relaxation**

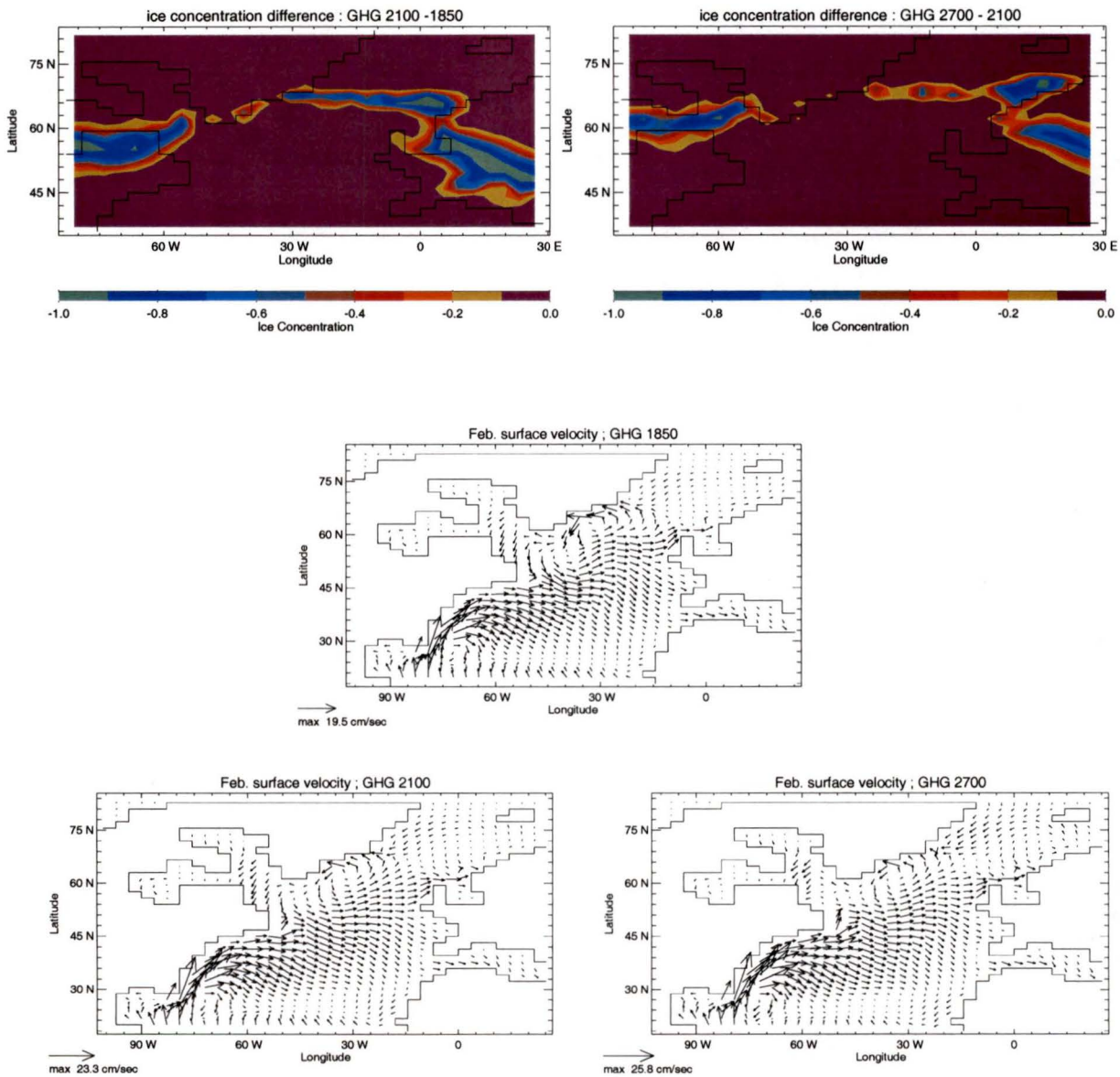

Figure 5.8: **February ice concentration differences and surface velocities, *GHG* for 1850, 2100 and 2700**

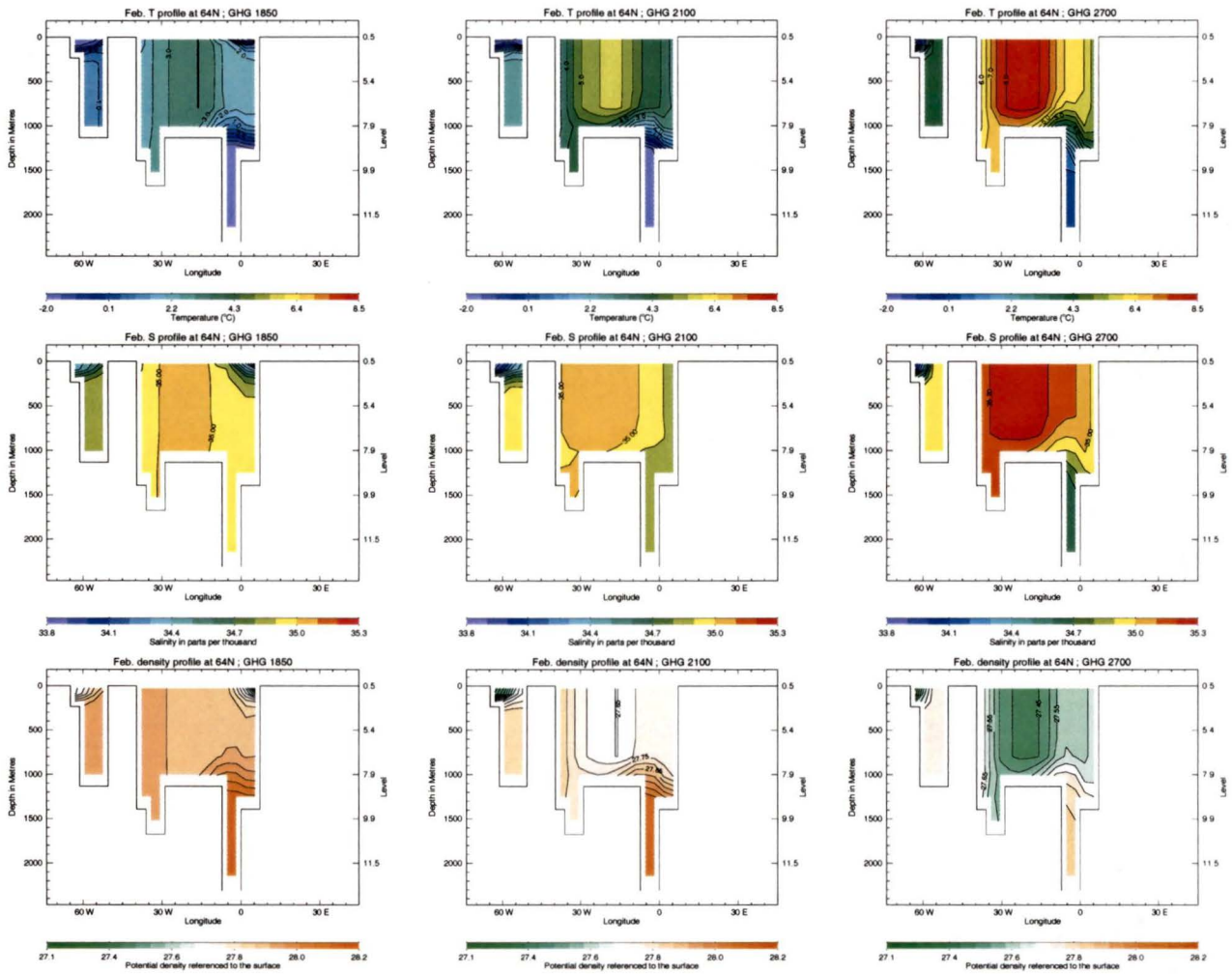

Figure 5.9: **Latitudinal profiles across 64°N of tempreature, salinity and density in *GHG* for 1850 (left), 2100 (centre) and 2700 (right)**

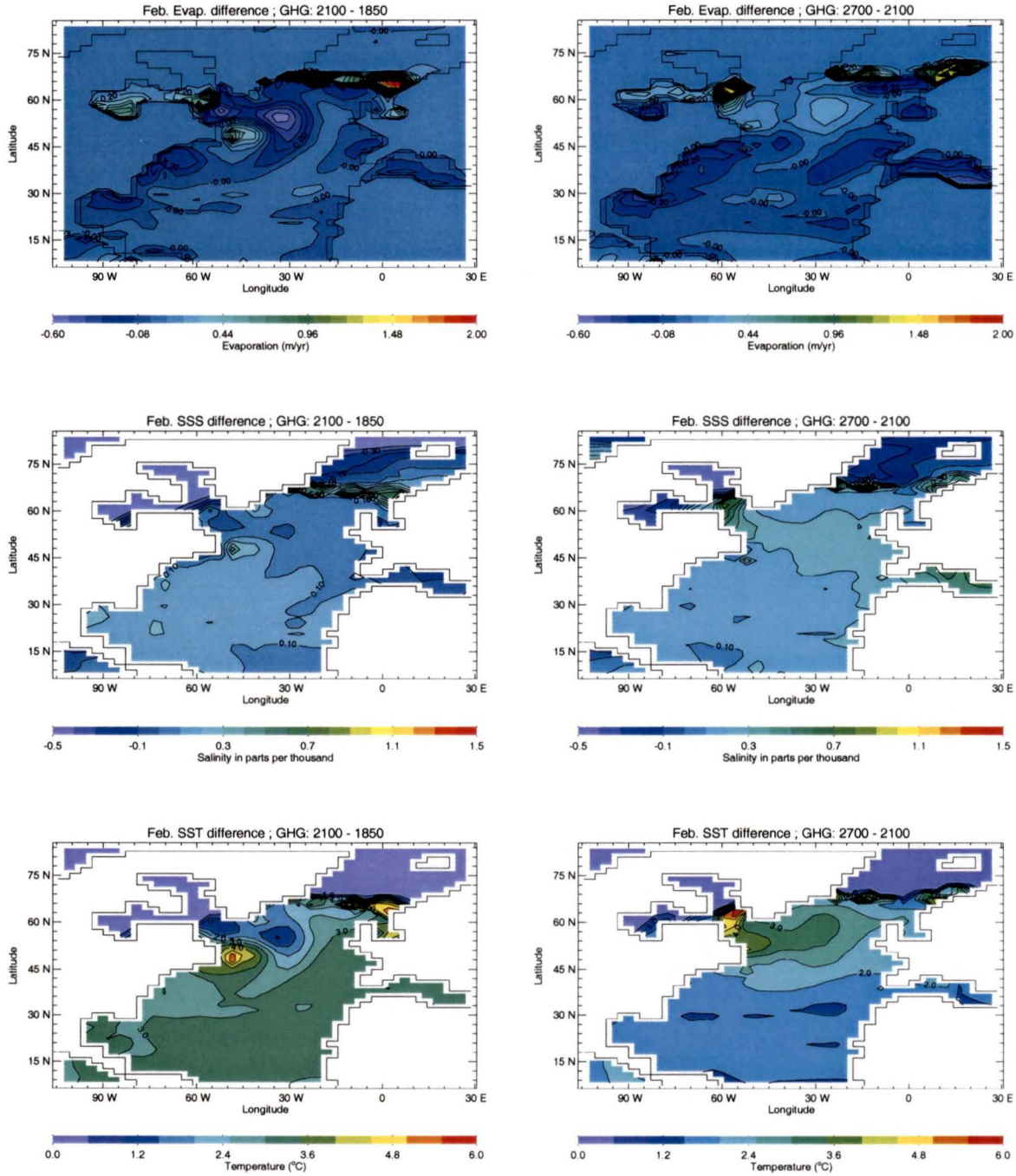

Figure 5.10: **Evaporation, SSS, SST differences in *GHG* between 1850 - 2100 (left) and 2100 - 2700 (right)**

Chapter 6

Conclusions

Over the last million years, the Earth has undergone a succession of glacial cycles with a periodicity of 100 ky. It is recognized that these oscillations are the result of variations in orbital parameters. However, understanding the exact relation between the gradual variations in incoming solar radiation and geological records of rapid climate changes is still a major issue in paleoclimatology. It is believed that internal feedbacks within the Earth system are the link between the external solar forcing and the different climate states. In particular, the ocean through its large heat capacity and slow circulation is a major regulator of the global climate and so could be part of this link.

In the current interglacial period, the mild climate over the North Atlantic region comes from warm tropical water being drawn northward to sites of deep water formation. The North Atlantic Deep Water (NADW) formation plays a major role in global climate. Understanding the causes and consequences of its variations is one key for the comprehension of the climate system and its intricate internal dynamics. The NADW is currently composed of two water masses: 1- the Lower NADW, originating from the Nordic Seas as Denmark Strait Overflow Water (DSOW), 2- the Upper NADW, seasonally formed in the Labrador Sea (LS) by convection processes and also named Labrador Sea Water (LSW). The rate of formation of these two water masses tightly governs the North Atlantic meridional overturning, hence the meridional heat transport responsible for regulating the present climate. Micropaleontological studies (Hillaire-Marcel et al. 2001, de Vernal et al. 2002) covering the last glacial cycle lead to the conclusion that there was no LSW formation during the last interglacial (Eemian : 125-118 kbp), which is thought to have been stable and warmer than today. They also suggest that the formation of deep water in the LS occurred for the first time a few thousand years after the deglaciation, around 8 kbp and had no anologues through the last glacial cycle. This supports the idea that the rate of deep water formation plays a major role in relating the gradual variations in external forcing with the abrupt changes between past climates.

Global warming projections predict a possible cessation of the LSW formation in a warm climate due to input of fresh water in this region through an enhanced hydrological cycle and sea ice melting (Wood et al. 1999). Thus with the perspective of future global warming,

studies of warm periods and past climate transitions become even more valuable.

In this thesis variations of LSW formation throughout the last glacial cycle were investigated using the UVic Earth System Climate Model. The model closely represents the present global ocean characteristics. The North Atlantic meridional overturning has a maximum value of 21 Sv, the meridional North Atlantic circulation cell is deep and has its core at 50°N. The NADW is formed by winter convection in the LS and in the Irminger Sea above the Iceland-Scotland Ridge. The convection in the Irminger Sea substitutes for the DSOW, which the model fails to represent due to its coarse resolution.

The experiments run with the UVic Earth System Climate model, representing different times during the last glacial cycle, indicate a great sensitivity of the NADW formation to the two radiative forcings, *i.e.* the orbital parameters and the atmospheric CO_2 concentration. From the last interglacial to global warming projections, the thermohaline circulation in the model varies significantly but never collapses.

In the Eemian simulation (*125K*) deep water formation is active only in the Irminger Sea and stops in the LS, in agreement with micropaleontological studies (Hillaire-Marcel et al. 2001). It leads to a low overturning of 15 Sv. In the Last Glacial Maximum simulation (LGM, 21 kbp), convection stops in the LS, and the Irminger site shifts southward to the Bay of Biscay, agreeing with the micropaleontological study of de Vernal et al. (2002). This single site of deep water formation produces a weak and shallow meridional North Atlantic circulation and a maximum North Atlantic overturning of 12 Sv. Experiments have also been conducted to represent the 12 kbp and 6 kbp period, with CO_2 concentrations ranging from 243 to 270 *ppm*. All of these experiments produce an oceanic circulation similar to the modern one even though greenhouse forcing is lower. These results do not fit with the paleo-reconstructions. However, in a long transient run with freshwater forcing added during the deglaciation, the overturning collapses at 17 kbp and resumes around 6 kbp to reach modern values. Finally, in the global warming experiments, as CO_2 increases, convection is still active in the Irminger Sea but stops in the LS, in agreement with another modelling study (Wood et al. 1999). The maximum North Atlantic meridional overturning decreases to 17 Sv as CO_2 increases to 1390 *ppm*. The meridional North Atlantic cell becomes shallower and its core shifts northward as CO_2 rises. Once CO_2 is held constant at high values, the system tends to an equilibrium where LS convection resumes and is associated with an increase in the meridional overturning, which reaches a maximum value of 25 Sv for $CO_2 = 1390$ *ppm*. The meridional cell is also shallower and its core is situated further northward to 55°N at higher CO_2 concentrations.

The experiments show a relative stability of the convection site on the east side of

the basin (Irminger Sea and Bay of Biscay). On the other hand, they demonstrate a great sensitivity of the LS convection to variations in both orbital parameters and CO_2 concentrations. The intensity of the thermohaline circulation is highly dependent on the LSW formation. It systematically decreases when the LS convection dies and increases when it resumes. The variations of LSW formation are caused by different reasons depending on the external forcings.

At 125 kbp, during the Eemian, the orbital parameters generate a more seasonally contrasted climate which allows extended seasonal sea ice in the confined environment of the LS, hence blocking the convection. At the same time the warm low latitudes still provide a relatively warm North Atlantic Drift reaching the Irminger Sea where it cools and forms the NADW. In the LGM run, the low CO_2 concentration of 200 *ppm* allows strong winter cooling and leads to a cold climate with extensive sea ice formation over the entire northern North Atlantic, insulating the ocean surface from the atmosphere and prohibiting convection processes. As a result deep water formation entirely ceases in the LS and the Irminger Sea. The North Atlantic Drift shifts southward along the ice edge, and the convection occurs in the Bay of Biscay. In the global warming experiments, the high CO_2 concentrations have a strong influence on NADW formation. In the transient warming states the warm North Atlantic drift penetrates further north-eastward, extending the site of convection in the Irminger Sea to the Nordic Seas. On the other hand, sea ice melting in the confined LS keeps its surface fresh, inhibiting convective processes. The North Atlantic circulation is slowed down and acts as a negative feedback to high latitude warming. However once the system is allowed to tend to an equilibrium, the fresh water lid in the LS disappears and the convection is restored, acting then as a positive feedback to high latitude warming.

The time periods without LSW formation (*i.e.* Eemian, LGM, global warming transient) experience a low meridional overturning compared to the current 21 Sv, which varies depending on the surface conditions generated by the external forcings. In the global warming experiments, the high temperatures at low latitude maintain a steep meridional depth-integrated steric height gradient responsible for the overturning of 17 Sv. In *125K*, representing the Eemian simulation, the contrasted climate generates large meridional temperature and salinity gradients, leading to a maximum overturning of 15 Sv, whereas in the cold LGM run, the cooler tropics reduce the meridional depth-integrated steric height gradient leading to the lower overturning of 12 Sv.

When convection in the LS remains active, different equilibria are defined. The variations in orbital parameters and CO_2 concentration in the Holocene simulations (12-6 kbp) are too small to modify the modern equilibrium. However they allow us to further constrain

the CO_2 threshold found by Yoshimori (2001) between glacial and modern modes from 200-280 *ppm* to 200-243 *ppm*. In the global warming experiments another CO_2 threshold is found. It stands between 350 to 600 *ppm* and separates the modern mode from a global warming mode which has a strong but shallow meridional overtuning cell.

The Holocene simulations also show that the perpetual forcing runs are adequate to simulate stable climates, such as glacial or modern modes, but fail in representing transient states. In order to simulate a transient state the right forcing has to be applied. For the deglacial transition, fresh water forcing from ice sheet melting is obviously fundamental. When it is applied, the meridional North Atlantic circulation reacts as expected from proxy reconstructions (*i.e.* collapses during the forcing and resumes afterward).

In summary, convection occurs through the cooling of the North Atlantic Drift water. The Irminger convection site is in direct contact with the North Atlantic Drift and is therefore relatively stable. The LS is far from the North Atlantic Drift source and receives its influence only via the Irminger current, which makes the LS surface very sensitive to fresh water flux variations. These variations can alternatively be induced by variations in orbital geometry, CO_2 concentrations or continental ice sheet melting. This set of simulations generally agrees with the paleo-reconstruction of Hillaire-Marcel et al. (2001) concerning the LSW formation occuring for the first time in the late Holocene with no analogues through the last glacial cycle, and with Wood et al. (1999) claiming a collapse of LS convection in a global warming situation. The differences between the glacial, interglacial and global warming modes under quasi-identical orbital parameters and various CO_2 concentrations, show different thermohaline circulation states inducing different climate conditions. This represents part of the mechanisms linking gradual orbital changes to abrupt climate changes.

Also, the difference between equilibrium and transient runs shows that the traditional method using perpetual forcing to evaluate models is only appropriate for the representation of stable climates states. Because of its large thermal inertia the ocean has a long-term memory and past climate states influence future ones. In order to have a sense of transitional climate states, which is the case for future global warming, transient runs are necessary. This supports the conclusion in Weaver et al. (2000) raising the importance of paleoclimatic simulations and questioning the accuracy of current modelling strategies not considering this long-term memory.

Finally, a global warming climate will induce changes in freshwater fluxes, particulary at high latitudes. As the LS is found to be very sensitive to freshwater forcing in the model simulation, it encourages observational studies to concentrate here in order to monitor a possible oceanic response to greenhouse gas warming. In particular, measuring deep

currents at the entrance (Cape Farewell) and exit of the LS could provide indications for thermohaline circulation changes.

Bibliography

J. F. Adkins, L. Boyle, E. A.and Keigwin, and E Cortijo. Variability of the North Atlantic thermohaline circulation during the last interglacial period. *Nature*, 390:154–156, 1997.

R. B. Alley, P. U. Clark, L. D. Keigwin, and R. S. Webb. Making sense of Millenial-Scale Climate Change. In P. U. Clark, R. S. Webb, and L. D. Keigwin, editors, *Mechanism of global climate change at millenial time scales*, volume 112 of *Geophysical Monograph*, pages 385–394. AGU, 1999.

J. M. Barnola, D. Raynaud, Y. S. Korotkevich, and C. Lorius. Vostok ice core provides 160,000 - years record of atmospheric CO_2. *Nature*, 329:408–414, 1987.

A. L. Berger. Long-term variations of daily insolation and Quaternary climatic changes. *J. Atmos. Sci.*, 35:2362–2367, 1978.

A. L. Berger and M.F. Loutre. Insolation values for the climate of the last 10 million years. *Quat. Sci. Rev.*, 10(4):297–317, 1991.

E. A. Boyle and L. Keigwin. North Atlantic thermohaline circulation during the past 20,000 years linked to high-latitude surface temperature. *Nature*, 330:35–40, 1987.

E. D. Boyle. Last-Glacial-Maximum North Atlantic Deep Water: On, Off or Somewhere in-between? *Philosophical Transactions of the Royal Society of London*, 347:243–253, 1995. Series B Biological Sciences.

W. S. Broecker. The biggest chill. *Natural History*, 96(10):74–82, October 1987.

W. S Broecker. The great ocean conveyor. *Oceanography*, 4:79 – 89, 1991.

W. S. Broecker. Massive iceberg discharges as triggers for global climate. *Nature*, 372: 421–424, 1994.

W. S. Broecker, G. Bond, M. Klas, G. Bonani, and W. Wolfli. A salt oscillator in the glacial northern Atlantic, 1. the concept. *Paleoceanography*, 5(4):469–477, 1990.

W. S. Broecker, G. Bond, M. Klas, E. Clark, and J. McManus. Origin of the northern Atlantic's Heinrich events. *Climate Dynamics*, 6:265–273, 1992.

W. S. Broecker and G. H. Denton. What drives glacial cycles? *Scientific American*, 262 (1):49–56, 1990.

P. U. Clark, R. B. Alley, and D. Pollard. Northern hemisphere ice-sheet influences onglobal climate change. *Science*, 286:1104–1111, 1999.

CLIMAP Project. *Seasonal reconstruction of the Earth's surface at the Last Glacial Maximum.* Map Chart Series, MC-36. Geological Society of America, Boulder, CO, 1981.

CLIMAP Project. The last interglacial ocean. *Quaternary research*, 21:123–224, 1984.

E. Cortijo, J. C. Duplessy, L. Labeyrie, H. Leclaire, J. Duprat, and T. C. E. van Weering. Eemian cooling in the Norwegian Sea and the North Atlantic Ocean preceeding ice-sheet growth. *Nature*, 1994.

E. Cortijo, S. Lehman, L. Keigwin, M. Chapman, D. Paillard, and L. Labeyrie. Changes in meridonal temperature and salinity gradients in the North Atlantic ocean (30°W-72°N) during the last interglacial period. *Paleoceanography*, 14(1):23–33, 1999.

T. J. Crowley. Temperature and circulation changes in the eastern North Atlantic during the last 150,000 years: evidences from the planktonic foraminiferal record. *Marine Micropaleontology*, 6:97–129, 1981.

T. J. Crowley and G. R. North. *Paleoclimatology*, volume 18 of *Oxford Monograph on Geology and Geophysics.* Oxford University Press, New York, NY, 1991.

W. B. Curry, J.-C. Duplessy, L. D. Labeyrie, and N. J. Shackleton. Change in distribution of δ^{13}C of deep water between the last glaciation and the Holocene. *Paleoceanography*, 3 (3):317–341, 1988.

W. Dansgaard, S. J. Johnsen, H. B. Clausen, D. Dahl-Jensen, N. Gundestrup, C. U. Hammer, and H. Oeschger. North Atlantic climatic oscillations revealed by deep Greenland ice cores. In J. E. Hansen and T. Takahashi, editors, *Climate processes and climate sensitivity*, volume 29 of *Geophysical Monograph*, pages 288–298. American Geophysical Union, 1984.

W. Dansgaard, S. J. Johnsen, S. B. Clausen, D. Dahl-Jensen, N. S. Gundestrup, C. U. Hammer, C. S. Hvidberg, J. P. Steffensen, A. E. Sveinbjornsdottir, J. Jouzel, and G. Bond. Evidence for general instability of past climate from a 250-kyr ice-core record. *Nature*, 364:218–220, 1993.

A. de Vernal, C. Causse, C. Hillaire-Marcel, R. J. Mott, and S. Occhietti. Palynostratigraphy and th/u ages of upper pleistocene interglacial and interstadial deposits on cap breton island, eastern canada. *Geology*, 14:554–557, 1986.

A. de Vernal and C. Hillaire-Marcel. Sea-ice, sea-surface salinity and the halo/thermocline structure in the northern North Atlantic: modern versus full glacial conditions. *Quaternary Science Reviews*, 19:65–85, 2000.

A. de Vernal, C. Hillaire-Marcel, W. R. Peltier, and A. J. Weaver. The structure of the upper water column in the northwest North Atlantic: Modern vs. Last Glacial Maximum conditions. *Paleoceanography*, 2002. in press.

A. de Vernal, A. Miller, and C. Hillaire-Marcel. Paleoenvironment of the last interglacial sensu lato in North Atlantic regions: eastern Canada and adjacent seas. *Quat Int.*, 10-12: 95–106, 1991.

J.-C. Duplessy, L. Labeyrie, M. Paterne, S. Hovine, T. Fichefet, J. Duprat, and M. Labracherie. High latitude deep water sources during the Last Glacial Maximum and the intensity of global oceanic circulation. In G. Wefer, W. H. Berger, G. Siedler, and D. J. Webb, editors, *The South Atlantic: Present and Past Circulation*, pages 445–460. Springer, Berlin Heidelberg, 1996.

J.-C. Duplessy, N. J. Shackleton, R. G. Fairbanks, L. Labeyrie, D. Oppo, and N. Kallel. Deepwater source variations during the last climatic cycle and their impact on the global deepwater circulation. *Paleoceanography*, 3(3):343–360, 1988.

R. G. Fairbanks. A 17,000-year glacio-eustatic sea level record: Influence of glacial melting rates on the Younger Dryas event and deep-ocean circulation. *Nature*, 342:637–642, 1989.

A. F. Fanning and A. J. Weaver. An atmospheric energy-moisture balance model: climatology, interpentadal climate change, and coupling to an ocean general circulation model. *J. Geophys. Res.*, 101(D10):15111–15128, 1996.

L.A. Frakes, J.E. Francis, and J.I. Syktus. *Climates Modes of the Phanerozoic.* Cambridge University Press, Cambridge, 1992.

H. Heinrich. Origin and consequences of cyclic ice rafting in northeast Atlantic ocean during the past 130,000 years. *Quaternary research*, 29:143 – 152, 1988.

III. W. D. Hibler. A dynamic thermodynamic sea ice model. *J. Phys. Oceanogr.*, 9(4): 815–846, 1979.

C. Hillaire-Marcel, A. de Vernal, G. Bilodeau, and A.J. Weaver. Absence of deep-water formation in the Labrador Sea during the last interglacial period. *Nature*, 410:1073–1077, 2001.

E. C. Hunke and J. K. Dukowicz. An elastic-viscous-plastic model for sea ice dynamics. *J. Phys. Oceanogr.*, 27(9):1849–1867, 1997.

J. Imbrie, E. A. Boyle, S. C. Clemens, A. Duffy, W. R. Howard, G. Kukla, D. J. Kutzbach, J. Martison, A. McIntyre, A. C. Mix, B. Molfino, J. J. Morley, L. C. Peterson, N. G. Pisias, W. L. Prell, M. E. Raymo, N. J. Shackteton, and Toggweiler J. R. On the structure and origin of major glaciation cycles, 1. linear responses to Milankovitch forcing. *Paleoceanography*, 7(6):701–738, 1992.

A. Indermühle, T.F. Stocker, F. Joos, H. Fischer, H.J. Smith, M. Wahlen, B. Deck, D. Mastroianni, J. Tschumi, T. Blunier, R. Meyer, and B. Stauffer. Holocene carbon-cycle dynamics based on CO_2 trapped in ice Taylor Dome, Antarctica. *Nature*, 398:121–126, 1999.

IPCC. *Climate Change 2001: The Scientific Basis.* Cambridge University Press, Cambridge, 2001.

T.-L. Ku, M. A. Kimmel, W. H. Easton, and T. J. O'Neil. Eustatic sea level 120,000 years ago on Oahu, Hawaii. *Science*, 183:959,962, 1974.

L. D. Labeyrie, J.-C. Duplessy, and P.L. Blanc. Variation in mode of formation and temperature of oceanic deep water over the past 125,000 years. *Nature*, 327:477–482, 1987.

S. J. Lehman and L. D. Keigwin. Sudden changes in the North Atlantic circulation during the last deglaciation. *Nature*, pages 757–762, 1992.

J. M. Licciardi, J. T. Teller, and P. U. Clark. Freshwater routing by the Laurentide ice sheet during the last deglaciation. In P. U. Clark, R. S. Webb, and L. D. Keigwin, editors, *Mechanisms of Global Climate Change at Millennial Time Scales*, number 112 in Geophysical Monograph Series, pages 177–201. American Geophysical Union, 1999.

T. S. Liu, Z. An, B. Yuan, and J Huan. The loess paleosol sequence in China and climatic history. *Episodes*, 8:21–41, 1985.

J. Lynch-Stieglitz, W. B. Curry, and N. Slowey. Weaker Gulf Stream in the Florida straits during the Last Glacial Maximum. *Nature*, 402:644–648, 1999.

S. Manabe and R. J. Stouffer. Two stable equilibria of coupled ocean-atmosphere model. *J. Climate*, 1:841–866, 1988.

S. Manabe and R. J. Stouffer. Century-scale effects of increased atmospheric CO_2 on the ocean-atmosphere system. *Nature*, 364:215–218, July 1993.

S. Manabe and R. J. Stouffer. The role of thermohaline circulation in climate. *Tellus*, "51 A-B":91–109, 1999.

M. S. McCartney and R. G. Curry. On the mid-latitude formation of lower North Atlantic deep water. *personal communication*, 2002.

K. J. Meissner and R. Gerdes. A coupled atmosphere-ocean-sea ice model. Part I: model description, simulation of an ice age initiation. *J. Geophys. Res.*, 2000.

E. Monnin, A. Indermühle, A Dallenbach, J. Fluckiger, B. Stauffer, T. F. Stocker, D. Raynaud, and J-M. Barnola. Atmospheric CO_2 contration over the last glacial termination. *Science*, 291:112–114, 2001.

R. C. Pacanowski. MOM 2: Documentation user's guide and reference manual. GFDL Ocean Group Technical Report 3.2, NOAA, GFDL, Princeton, NJ, November 1996. 329pp.

C. L. Parkinson and W. M. Washington. A large-scale numerical model of sea ice. *J. Geophys. Res.*, 84(C1):311–337, 1979.

W. R. Peltier. Mantle viscosity and ice-age ice sheet topography. *Science*, 273:1359–1364, 1996.

J. R. Petit, J. Jouzel, D. Raynaud, N. I. Barkov, J. M. Barnola, I. Basile, M. Bender, J. Chappellaz, M. Davis, G. Delaygue, M. Delmotte, V. M. Kotlyakov, M. Legrand, V. Y. Lipenkov, C. Lorius, L. Pepin, C. Ritz, E. Saltzman, and M. Stievenard. Climate and atmospheric history of the past 420,000 years from the Vostok ice core, Antarctica. *Nature*, 399:429–436, 1999.

N. Petit-Maire. Paleoclimate in the Sahara of Mali: A multidisciplinary study. *Episodes*, 9:7–16, 1986.

E. M. Pokras and A. C. Mix. Eolian evidence for spacial variability of late Quaternary climates in tropical Africa. *Quaternary Research*, 24:137–149, 1985.

W. L. Prell and J. E. Kutzbach. Monsoon variability over the past 150,00 years. *J. Geophys. Res.*, 92:8411–8425, 1987.

S. Rahmstorf. A fast and complete convection scheme for ocean models. *Ocean Modelling*, 101:9–11, 1993.

S. Rahmstorf. Decadal variability of the thermohaline ocean circulation. In A. Navarra, editor, *Beyond El Niño: Decadal Variability in the Climate System*, pages 329–351. Springer, 1999.

T. L. Rasmussen, E. Thompsen, van Weering T. C. E., and L. Labeyrie. Rapid changes in surface and deep water conditions at the Faeroe margin during the last 58,000 years. *Paleoceanography*, 11(6):757–772, 1996.

S. R. Rintoul. South Atlantic interbasin exchange. *J. Geophys. Res.*, 96:2675 – 2692, 1991.

D. Roemmich and C. Wunsch. Two transatlantic sections: Meridional circulation and heat flux in the subtropical North Atlantic Ocean. *Deep-Sea Res.*, 32(6):619–664, 1985.

A. Rosell-Melé. Appraisal of climap temperature reconstruction in the NE Atlantic using alkenone proxies. *EOS*, 78(46):F28, 1997.

R. L. Rutberg, S. R. Hemming, and S. L. Goldstein. Reduced North Atlantic deep water flux to the glacial southern ocean inferred from neodymium isotope ratios. *Nature*, 405: 935–938, 2000.

C. Sancetta, J. Imbrie, and N.G. Kipp. Climatic record of the past 130,000 years in the North Atlantic deep sea core V23-32: correlation with the terrestrial records. *Quaternary Reasearch*, 3:110 – 116, 1973.

M. Sarnthein, K. Winn, S. J. A. Jung, J.-C. Duplessy, L. Labeyrie, H. Erlenkeuser, and G. Ganssen. Changes in East Atlantic deepwater circulation over the last 30,000 years: Eight time slice reconstructions. *Paleoceanography*, 9(2):209–267, 1994.

A. Schmittner, K.J. Meissner, M. Eby, and A.J. Weaver. Forcing the deep ocean circulation in simulations of the Last Glacial Maximum. *Paleoceanography*, 17:5:1–5:15, 2002a.

A. Schmittner, M. Yoshimori, and A.J. Weaver. Instability of glacial climate in a model of the ocean-atmosphere-cryosphere system. *Science*, 295:1489–1493, 2002b.

D. Seidov, M. Sarnthein, K. Stattegger, R. Prien, and M. Weinelt. North Atlantic Ocean circulation during the Last Glacial Maximum and subsequent meltwater event: A numerical model. *J. Geophys. Res.*, 101:16305–16332, 1996.

A. J. Jr. Semtner. A model for the thermodynamic growth of sea ice in numerical investigations of climate. *J. Phys. Oceanogr.*, 6(3):379–389, 1976.

T. F. Stocker and A. Schmittner. Influence of CO_2 emission rates on the stability of the thermohaline circulation. *Nature*, 388:862–865, 1997.

M. Stuiver and P.J. Reimer. Extended ^{14}C database and revised CALIB radiocarbon calibration program. *Radiocarbon*, 35:215–230, 1993.

A.J. Weaver, P. Duffy, M. Eby, and E. Wiebe. Evaluation of ocean and climate model using present-day observations and forcing. *Atmosphere-Ocean*, 38.(2):271–301, 2000.

A.J. Weaver, M. Eby, E. Wiebe, C. Bitz, P. Duffy, T. Ewen, G. Fanning, M. Holland, MacFadyen A., O. Saenko, A. Schmittner, H. Wang, and M. Yoshimoro. The UVic Earth system climate model:model description, climatology, and applications to past, present and future climates. *Atmosphere-Ocean*, 39 (4):361–428, 2001.

J. W. C. White. don't touch that dial. *Nature*, 364:186, 1993.

E. C. Wiebe and A. J. Weaver. On the sensitivity of global warming experiments to the parameterisation of sub-grid scale ocean mixing. *Climate Dynamics*, 15(12):875–893, 1999.

R.A. Wood, Keen. A.B., J.F.B. Mitchell, and J.M. Gregory. Changing spatial structure of the thermohaline circulation in response to atmospheric CO_2 forcing in a climate model. *Nature*, 399:572–575, 1999.

L. V. Worthington. The Norwegian Sea as a mediterranean basin. *Deep–Sea Res.*, 17:77 – 83, 1970.

M. Yoshimori. *Modelling Studies of Glacial-Interglacial Transitions.* PhD thesis, University of Victoria, 2001.

E.-F. Yu, R. Francois, and M. P. Bacon. Similar rates of modern and last-glacial ocean thermohaline circulation inferred from radiochemical data. *Nature*, 379:689–694, 1996.

R. Zanh, J. Schonfeld, H. R. Kudrass, M. H. Park, and P. Erlenkeuser, H.and Grootes. Thermohaline instability in North Atlantic during melt-water events: Stable isotope and ice-rafted records from core SO75-26KL, Portugese margin. *Paleoceanography*, 12(5): 696–710, 1997.

VITA

Personal Data:

Surname:	Cottet
Given Name:	Melanie
Place of Birth:	Echirolles, France

Educational Institutions Attended:

Université Joseph Fourier, Grenoble	1993-1996
Université du Québec à Montréal	1996-1997
Université Bordeaux I	1997-1998
Université Joseph Fourier, Grenoble	1998-1999

Degrees Awarded:

Bachelor of Geology	Université Joseph Fourier	1997
Master of Oceanography	Université Joseph Fourier	1999

Publications:

S. Gulev, B. Barnier, H. Knochel, J-M Molines and M. Cottet (2002): Water mass transformation in the North Atlantic and its impact on the meridional circulation: insights from an ocean model forced by NCEP/NCAR reanalysis surface fluxes. *Journal of Climate*, in revision.

University of Victoria
Partial Copyright License

I hereby grant the right to lend my dissertation to users of the University of Victoria Library, and to make single copies only for such users or in response to a request from the Library of any other university, or similar institution, on its behalf or for one of its users. I further agree that permission for extensive copying of this dissertation for scholarly purposes may be granted by me or a member of the University designated by me. It is understood that copying or publication of this dissertation for financial gain shall not be allowed without my written permission.

Title of Dissertation: VARIATION OF DEEP WATER FORMATION IN THE LABRADOR SEA OVER THE LAST GLACIAL CYCLE (130 KY) AND IN FUTURE CLIMATE MODEL PROJECTIONS.

Author: [redacted]

Melanie Cottet

2002 June